STRESS ANALYSIS OF A DOUBLE-DOUBLER JOINT
IN COMPOSITE STRUCTURE

By

MYUNG KYUN PARK

A DISSERTATION PRESENTED TO THE GRADUATE SCHOOL
OF THE UNIVERSITY OF FLORIDA IN PARTIAL FULFILLMENT
OF THE REQUIREMENTS FOR THE DEGREE OF
DOCTOR OF PHILOSOPHY

UNIVERSITY OF FLORIDA

1990

ACKNOWLEDGEMENTS

TABLE OF CONTENTS

APPENDICES

LIST OF TABLES

vi

LIST OF FIGURES

vii

x

Abstract of Dissertation Presented to the Graduate School
of the University of Florida in Partial Fulfilment of
the Requirements for the Degree of Doctor of Philosophy

STRESS ANALYSIS OF A DOUBLE-DOUBLER JOINT
IN COMPOSITE STRUCTURE

BY

MYUNG KYUN PARK

May, 1990

Chairman: Lawrence E. Malvern
Major Department: Aerospace Engineering,
                  Mechanics and Engineering Science

This study first provides a linear elastic stress
analysis using the finite element method for a double-doubler
adhesive joint. The joint is modelled such that the variation
of stresses and strains through the adhesive thickness can be
determined. The linear elastic stress analysis is focused on
three areas: first, the interfacial stress distribution
between the adherend and adhesive; second, cohesive stress
distribution in the adhesive; and third, stress distribution
across the thickness of the adhesive layer at the ends of
layer.

The second step is to carry out a parametric study on
the double-doubler joint. Since the stress distribution in
the adhesive layer depends on several parameters (geometrical

and material), an understanding of the influence of these various parameters will lead to better joint design for specific requirements.

The third step is to devise parameters that describe the singular behavior near the bonding edges between the adherend and the adhesive layer by applying the existing elastic solution for stress singularities to the double-doubler joint problem. The specified boundary displacement method is then used to determine the values of parameters. These parameters can be used as a means of failure prediction by comparing the calculated parameters with known critical values of the parameters for the material and comparison of stresses very near the bonding corners where stress singularities occur.

CHAPTER 1
INTRODUCTION

1.1 Introduction

In the design of material structures components must be joined in such a manner that overall the structure retains its structural integrity while performing its intended function subjected to loads and environment. Joining metallic structures is a well-developed technology involving riveting, bolting, welding, glueing, brazing, soldering, and combinations thereof. However, for polymer matrix fiber reinforced composites only adhesive bonding and mechanical fasteners (bolts and rivets) can be utilized.

Recent advances in composite structures and the new adhesive bonding techniques based upon very strong epoxy type adhesives have made feasible the adhesive joining, stiffening and repairing of structural elements subjected to extreme enviromental and loading conditions. This type of joining and stiffening has been used in the aerospace, automobiles, electronics, sporting goods and appliance industries. Consequently the importance of adhesive bonding in technology has been recognized. Various types of adhesive joints are shown in Figure 1.1. Among the various types of joints, the double-doubler joint is selected for this study.

1

Adhesive bonding provides structures having lighter weight, more fatigue resistance, improved aerodynamic smoothness, better distribution of imposed stress, better thermal and electrical insulation and greater crack retardance over mechanical fasteners. Therefore, adhesive bonding is very desirable for use in composite material structures.

The use of adhesives is growing rapidly but designers lack the definitive approach that gives confidence in routinely incorporating adhesive bonding into design.

1.2 Objective and Scope

The analysis of the behavior and the failure of an adhesive joint must include both the understanding of the mechanism of adhesion, which is closely related to the microstructure between the adhesive polymer and the adherends, and the analysis of stresses in the joint. This study will be focused on the latter part. Failure in an adhesive joint can be either "adhesive," which occurs at the interfaces between the adhesive and the adherend, or "cohesive," which occurs either in the adhesive or in the adherends.

Therefore the first objective of this thesis is to do a linear elastic stress analysis for the double-doubler joint by means of finite element method (using ANSYS). The linear elastic stress analysis is focused on three areas: first, the interfacial stress distribution between the adherend and the adhesive; second, cohesive stress distribution in the

adhesive; and finally, the stress distributions at various levels of y in the adhesive layer near the ends of layer.

The second objective is to carry out a parametric study on the double-doubler joint. Since the stress in the adhesive layer depends on several parameters (geometrical and material), an understanding of the influence of these various parameters will lead to better joint design for specific requirements.

The third objective is to devise parameters that describe the singular behavior near the bonding edges between the adherend and the adhesive layer by applying an existing elastic solution for stress singularities to the double-doubler adhesive joint problem. The specified boundary displacement method (SBD) is used to devise the parameters. These parameters can be used as a means of failure prediction by comparing the calculated parameters with known critical values of these parameters for the material and comparison of stresses very near the bonding corners where stress singularities occur.

Single Lap Joint

Double Lap Joint

Single Doubler Joint

Double Doubler Joint

Stepped Lap Joint

Scarf Joint

Figure 1.1 Various types of joints

CHAPTER 2
REVIEW OF PREVIOUS WORK

2.1 Introduction

A considerable amount of experimental and theoretical research has been carried out on adhesive bonded joints. Theoretical and experimental stress analyses of various types of adhesive-bonded joints have been made by many authors. Due to the relatively simple geometry and wide application, many theoretical and experimental analyses have been devoted to the single lap joint. (See Figure 2.1)

In this review the important investigations of the single lap joint and known investigation of the double lap joints are included. The following review provides a history and background of the present state of knowledge in adhesively bonded joints. First the investigations of the single-lap joint are reviewed here because the earlist analyses and the analyses which are used as the basis for most subsequent analyses were made on the single-lap joint.

The terminology used in identifying various parts of the joint is shown for a single lap joint in Figure 2.2. The "overlap" is the length over which the adhesive extends, and the "overhang" is the part of the adherend outside the overlap. The adhesive layer has two interfaces and two free

5
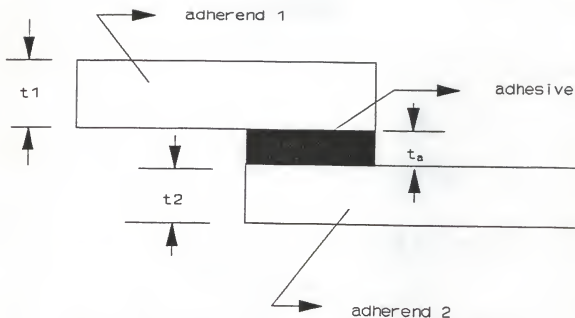
Figure 2.1 The single lap adhesive bonded joint
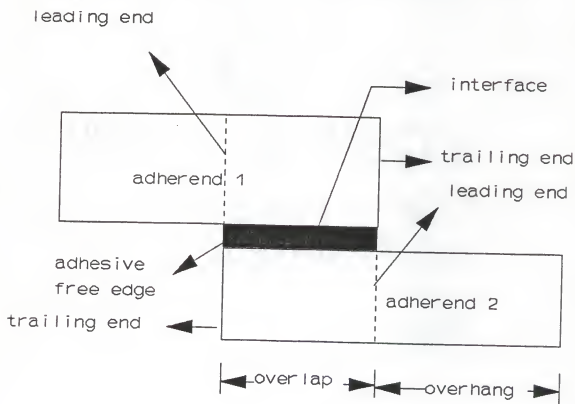
Figure 2.2 Identification of the various parts
of a single lap joint

edges. The "leading end" of an adherend is where the overhang begins after the overlap. The "trailing end" of the same adherend is at the opposite end of the overlap. Corresponding parts of the double-lap joints are identified with the same terminology. A typical single-lap joint is under tensile loading.

2.2 Analytical Studies

2.2.1 Volkersen's Theory

Classical analysis of an adhesive bonded joint was made by Volkersen [1]. He derived the load distribution of a multi-row riveted lap joint in tension, where he idealized the rivets by replacing them by a continous medium of given shear flexibilty, and considered the case of an adhesive bond. Bending of the adherends and the associated lateral normal and axial normal stresses were not considered. Therefore the shear stress was forced to be constant through the thickness of adhesive. By setting up the differential equations of linear elasticity, he showed that shear stress at any point along the length of the overlap was given with respect to dimensionless quantites:

a) the overlap ratio

$$D = Gc^2/E_2 t_a t_2 \qquad 2.1$$

b) the adherend stiffness

$$W = \left(\frac{E_1 t_1 + E_2 t_2}{E_1 t_1} \right) \qquad 2.2$$

The shear stress distribution in the adhesive layer was nonuniform in the x-direction, but assumed uniform constant in the y-direction. Peaks of the shear stress occurred at the ends of the overlap. He compared the maximum shear stress, τ_{max} at the ends of the overlap with the mean stress, τ_m and found the stress concentration factor, η_1 , for joints with nonidentical adherend.

$$\eta_1 = \frac{\tau_{max}}{\tau_m} = (D/W)^{1/2} \frac{(W-1)\cosh[(DW)^{1/2}]}{\sinh[(DW)^{1/2}]} \qquad 2.3$$

where $D = Gc^2/E_2t_2t_a$

$W = (E_1t_1+E_2t_2)/E_1t_1$

τ_m = averaged applied shear stress

This is for the case $E_1t_1 > E_2t_2$. He showed that the stress concentration factor increased with increasing shear modulus of the adhesive and with decreasing moduli of elasticity and thickness of the adherends.

The theory developed by Volkersen has two important shortcomings.

a) The bending deformation was neglected. (There should be a bending moment applied to the joint in addition to the in-plane tension, since the two applied forces are not collinear.)

b) The assumption was made that the shear stress does not vary across the thickness.

2.2.2 Goland and Reissner Theory

Goland and Reissner [2] studied the stress distribution for adhesive joints with identical adherends under the action of tensile forces at the ends of the adherends. The forces act in the direction parallel to the bonding line before any deformation takes place, but the line of action of the tensile force R is assumed to pass through the midpoint of the adhesive layer for the deformed equilibrium configuration. They recognized that the bending of the adherends beyond the bonded region has a significant effect on the stress distributions in the joint itself. They approached the problem in two steps. First they determined the loads at the edges of the joint which were transmitted from the loads at the ends of the adherends. In the first step of the problem, they treated the adherends as cylindrically bent plates, and found that forces transmitted to the edges of the joint consisted of a tensile force P, a small shear force V, and a bending moment M, as shown in Figure 2.3 in which

$$P \approx R$$
$$V = KP[3(1 - \nu_1{}^2)P/E_1t_1]^{1/2} \qquad 2.4$$
$$M = KPt_1/2$$
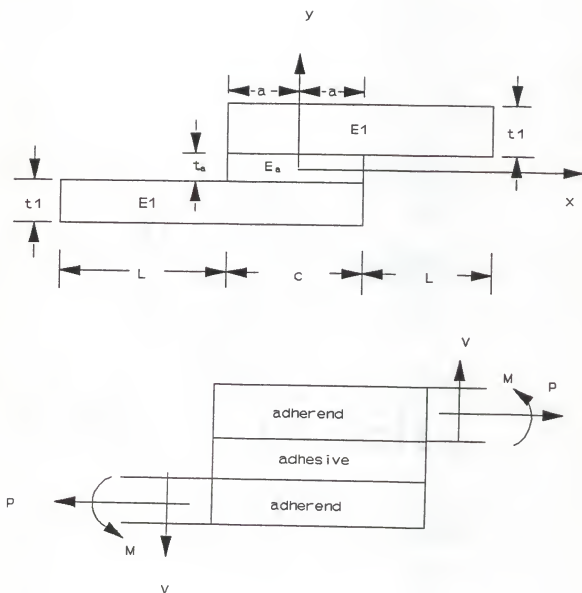
Figure 2.3 Systems considered by Goland and Reissner

where K is the bending moment factor which is the ratio of the magnitude of the edge moment M and the value of this moment in a nondeformable system:

$$K = \cfrac{1}{1+(2\sqrt{2})\tanh[\,(c/4t_1)\sqrt{6(1-\nu^2_1)P/E_1t_1}\,]}$$ 2.5

The value K=1 indicates that the adherends exhibit no deformation due to bending, and K < 1 indicates that a certain amount of bending deformation takes place.

In the second step of the problem, they assumed that the normal stress in the adhesive parallel to the layer can be neglected, and that the lateral normal stress and shear stress do not vary across the thickness of the adhesive layer. They used a plane strain analysis and solved the problem for two limiting cases:

1) The case where the adhesive layer is so thin and stiff that its deformation may be neglected. This case requires that the condition $t_a/E_a \ll t_1/E_1$. The results show that, while the lateral normal stress is high at the edge of the joint, the shear stress is zero there. The shear stress, however, rises rapidly to a maximum value in close proximity to the edge.

2) The case in which the adhesive layer is soft and flexible and the joint flexibility is mainly due to the

deformation of the adhesive layer. This case requires the condition $t_a/E_a \gg t_1/E_1$. The shear stress τ and lateral normal stress σ are expressed as follows.

$$\tau = \frac{p}{4c} \quad [\ \frac{\beta c}{2t_1} \ (1+3K) \ \frac{\cosh(\beta x/t_1)}{\cosh(\beta c/2t_1)} \ + \ 3(1-K) \ ] \qquad 2.6$$

$$\sigma = (1/\Delta)(P/t_1)(2t_1/c)^2 \ [\ (R_2\lambda^2 \ K/2 \ +$$
$$\lambda K' \cosh\lambda \ \cos\lambda) \cosh(2\lambda x/c) \ \cos(2\lambda x/c) \qquad 2.7$$
$$+ \ (R_1\lambda^2 K/2 + \lambda K' \sinh\lambda \ \sin\lambda) \sinh(2\lambda x/c) \ \sin(2\lambda x/c)]$$

where

$$\beta = (8Gt_1/ \ E_1 t)^{1/2}$$
$$\lambda = (c/2t_1)(6Et_1/E_1 t)^{1/4}$$
$$R_1 = \cosh\lambda \ \sin\lambda + \sinh\lambda \ \cos\lambda$$
$$R_2 = \sinh\lambda \cos\lambda - \cosh\lambda \sin 1\lambda$$
$$\Delta = (1/2)(\sinh2\lambda + \sin2\lambda)$$
$$K' = Vc/2Pt_1$$

The maximum value of τ and σ are found at the edges of the joint.

$$\frac{\tau_{max}}{(P/t_1)} \ (\ \frac{c}{t_1} \ ) \ = \ \frac{1}{4} \ [\ \frac{\beta c}{2t_1} \ (1+3K) \ \coth \frac{\beta c}{2t_1} + \ 3(1-K) \ ] \qquad 2.8$$

$$\frac{\sigma_{max}}{(P/t_1)} \ (\ \frac{c}{2t_1} \ )^2 \ = \ \frac{\lambda^2 K}{2} \ \frac{\sinh2\lambda - \sin2\lambda}{\sinh2\lambda + \sin2\lambda} + \ \lambda K' \frac{\cosh2\lambda + \cos2\lambda}{\sinh2\lambda + \sin2\lambda}$$

$$2.9$$

Compared with the factor D used by Volkersen, it can be seen that $\beta c/2t_1 = (2D)^{1/2}$. For large values of D, $\coth(2D)^{1/2}$ approaches the value of 1, and therefore the shear stress concentration factor, η_1, can be written, for large D, as

$$\eta_1 = \tau_{max}/(p/c) \approx (1/4)(1+3K)(2D)^{1/2} + 3(1-K)/4 \qquad 2.10$$

where $D = Gc^2/E_2t_2t_a$

The limitations of Goland and Reissner theory include

    a) It is valid only for identical adherends.

    b) It is valid only for two special cases; the first case is for $t_a/E_a \ll t_1/E_1$, while the second case requires that $t_a/E_a \gg t_1E_1$.

    c) The stress across the adhesive layer thickness is assumed to be constant, which results in inaccurate predictions in the region adjacent to the edges of the overlap.

2.2.3 Plantema's Analysis

Plantema [3] combined the Goland-Reissner theory with Volkersen's theory in the analysis of a single-lap adhesive bonded joint. The factor K from the Goland-Reissner theory was employed to calculate the differential strain of the members due to bending, while Volkersen's theory was used to

calculate the differential strain of the members due to shear, and the stress at the edges of the overlap.

The shear stress concentration factor was given as

$$\eta_1 = [D(1+3K)/2]^{1/2}\coth[D(1+3K)/2]^{1/2} \qquad 2.11$$

He did not make an attempt to calculate the lateral normal stress.

2.2.4 Kelsey and Benson Theory

Kelsey and Benson [4] employed the complementary energy method to determine the shear and lateral normal stresses in a single lap joint. A linear variation of the lateral normal stress was allowed across the the adhesive layer, while the shear stress was assumed constant across the adhesive thickness. The result was a differential equation of higher order than that obtained by Volkersen, which enabled the boundary condition of zero shear stress at the ends of the overlap to be satisfied. The shear and lateral normal stress obtained are as follows:

Let $A = pm_1m_2c$

$D = (m_1\cosh m_1c/2)(\sinh m_2c/2)-(m_2\sinh m_1c/2)(\cosh m_2c/2)$

$\tau = (A/4D)[(\cosh m_1x)(\cosh m_2c/2)-(\cosh m_1c/2)(\cosh m_2x)]$

$$2.12$$

$$\sigma = (At/8D)[(m_1 sinh m_1 x)(cosh m_2 c/2)-(m_2 cosh m_1 c/2)(sinh m_2 c/2)]$$

2.13

The shear stress concentration factor $\eta = \tau/(p/c)$ is given by

$$\eta = \frac{m_1 m_2 c^2 (cosh m_1 (xc/2))(cosh m_2 c/2)(cosh m_1 c/2)(cosh m_2 (xc/2))}{4 \ m_1 (cosh m_1 c/2)(sinh m_2 c/2)-m_2 (sinh m_1 c/2)(cosh m_2 c/2)}$$

2.14

where

$$m_1 = \frac{6E_a}{Gt_a^2} (1 + m_3)$$

$$m_2 = \frac{6E_a}{Gt_a^2} (1 - m_3)$$

$$m_3 = (1 - \frac{2G^2 t_a}{3E_a E_1 t_1})^{1/2}$$

Kelsey and Benson imposed the zero shear stress boundary condition which causes a sharp drop of shear stress from its peak value at positions very near the ends to zero at ends. They reasoned that this is necessary for equilibrium because the adhesive/air boundary can not sustain a shear stress.

2.2.5 Pahoja's Analysis

Pahoja [5] made the analysis of the joint under tensile, shear, and bending loads as shown in Figure 2.4. The joint was subjected to a general loading condition. He employed the theory of minimum potential energy to study the axial normal,

lateral normal and shear stresses in the adhesive layer. He defined the displacements in the adhesive in terms of polynominals with m terms for the displacements in the x direction and n terms for the displacement in the y direction. The total energy was expressed in terms of the displacement components in series form. By minimizing the total potential energy of the system, a system of governing linear ordinary differential equations and natural boundary conditions were obtained. The equations were reduced to algebraic and first order differential equations by substituting new variables for the displacements and their derivatives. By solving these equations numerically, the stress distribution and stress concentrations were found. The stress concentrations for identical adherends have the follwing forms:

Shear stress

$$(\tau_{max}/\tau_{av}) = 1 + (6/7)[(19/18) - V_{\ell}](S_{\ell} - 1)$$
$$\text{for } V_{\ell} < 1 \text{ and } S_{\ell} > 4$$

2.15

$$(\tau_{max}/\tau_{av}) = -1 + (18/19)(V_{\ell} - 17/18)(S_{\ell} - 1)$$
$$\text{for } V_{\ell} > 1 \text{ and } S_{\ell} > 5$$

Lateral normal stress

$$(\sigma_y)_{max}/\tau_{av} = (t_2/c)(1.4 - 1.675 V_{\ell}) N_{\ell}^2$$

2.16
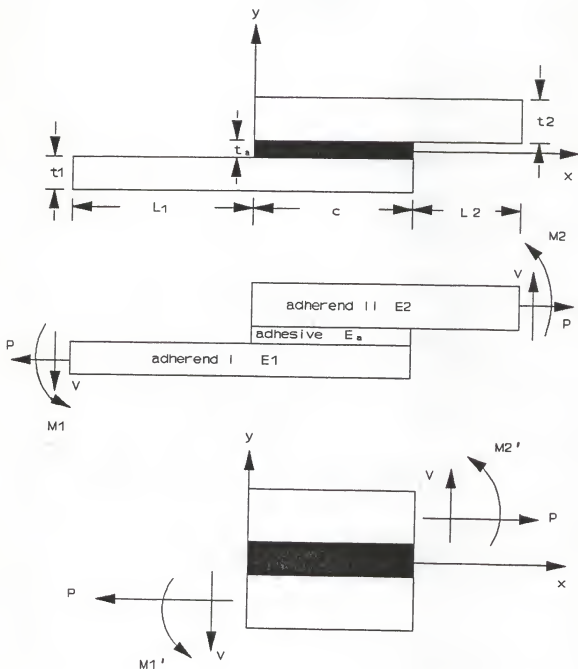
Figure 2.4 The single lap joint
analyzed by Pahoja

Axial normal stress

$$(\sigma_x)_{max}/\tau_{av} = (t_1/c)(0.85 - 0.95V_f) \ N_f^2 \qquad 2.17$$

where

$$V_f = \frac{V}{T} \qquad \frac{c}{[t_a + Q_1 \ t_1^2 \ \dfrac{(t + (4/3)t_1]}{\psi}}$$

$$S_f = (c/t_1)(Et_1/Et_a)^{1/2}$$

$$N_f = (c/t_1)(Et_a/E_1t_a)^{1/4}$$

$$Q_1 = E_1/(1-\nu_1^2)$$

$$\psi = Qt_a^2/6 + Q_1t_1t_a + Q_1t_1^2$$

$$Q = E/(1-\nu^2)$$

Pahoja concluded that the single lap joint with identical adherends was the best design. This joint was most efficient when loaded such that the shear stress distribution was uniform, i.e., $V_f = 1$. He compared his theoretical results with the results of photoelastic analysis, and these are in good agreement. The limitation of this analysis is that the free boundary condition at the ends of the adhesive were violated just as in Volkersen's and Goland and Reissner's analyses.

2.2.6 Renton and Vinson's Analysis

Renton and Vinson [6,7] made the most complete analysis of a single lap joint. They clearly identify the extent of the influence of the various parameters on the stress distribution in the adhesive and adherends. The analysis was very general and applicable to isotropic and anisotropic adherends as well as to dissimilar and similar adherends. The method of analysis that they developed involve the following assumptions and/or limitations:

1) The laminated adherends are symmetric about their own midsurfaces (i.e., no bending stretching coupling).

2) Each ply or lamina in each adherend is orthotropic

3) The effective elastic mechanical properties of the adhesive are accounted for.

4) Both shear and lateral normal stresses are accounted for in the adhesive; they vary in the load direction, but do not vary in the thickness direction.

5) The adhesive thickness is much smaller than the adherend thickness, i.e., $t_a \ll t_1$ and $t_a \ll t_2$

6) Shear deformation and lateral normal strains are accounted for in each adherend.

Composite material laminated plate theory was used as the building block or starting point for developing the method of analysis. The lap joint structure was divided into five portions for analysis: the adhesive, the adherends on either

side of the adhesive, and the adherend portions from the end of lap joint to the load application. Twenty-six boundary conditions are specified and satisfied.

The analytical solutions obtained for stresses and deformations throughout the structure were programmed on computer for easy calculation. After developing a valid closed form solution for the single lap joint problem, they ascertained the influence of certain important parameters on the stress distributions in the adhesive.

The influence of the joint parameters on the stress distributions in the adhesive are summarized below:

1) The greater the difference in the moduli of the adherends, the higher is the magnitude of the maximum shear stress.

2) For dissimilar adherends, the maxima of both the shear and the lateral normal stresses in the adhesive occured at the leading end of the less rigid adherend.

3) The greater the ratio of the moduli of the adherend and the adhesive, the more uniform the shear stress distribution.

4) The larger the ratio of the moduli of the adherends and the adhesive, the smaller is the magnitude of the maximum lateral normal stress.

In the design of single lap adhesive bonded joints, they recommended that

1) The adherends of joints should be identical.

2) The modulus of the adherends should be high compared to that of adhesive.

3) The length of overlap should be about ten times the minimum thickness of the adherend.

4) The joint's intended function should influence adhesive selection: in static bodies, adhesive ultimate strength should be high; in fatigue, adhesive fracture toughness should be considered.

2.2.7 Hart-Smith's Analysis

The analysis of a double lap joint by Hart-Smith [8] was designed to calculate the joint efficiency of a double lap joint in terms of the strength of the joint.

The adhesive was characterized as elastic-plastic in shear. In the analysis, the shear stress distribution was constant across the adhesive thickness.

In his analysis, the deformation of the adhesive was greatest at the ends of the overlap, and consequently the behavior of the adhesive was characterized as plastic at the ends of the lap.

In the elastic analysis, the shear stress in the adhesive was expressed in terms of the displacements in the outer and center adherends. The differential equation governing the

shear stress distribution was determined from the stress strain relationship and the force-equilibrium equation.

In the elastic-plastic analysis, the plastic shear stress and the distance over which the adhesive was plastic were determined from the boundary condition for the plastic region, the equation ensuring the continuity of the elastic and plastic shear strains, and the gross horizontal equilibrium equation of the joint. The expression for the plastic shear stress was then rearranged to express the applied load in terms of the shear strain energy per unit area of the adhesive layer.

The lateral normal stress in the adhesive was considered to be independent of the shear stresses. The analysis for the lateral normal stress was applicable only when the adhesive was deformed beyond the elastic range in joints with long overlaps. The lateral displacement of the outer adherends was related to the moment at the ends of the overlap by the theory of bending of plates.

The coefficients of the normal displacements, which were expressed in terms of trigonometric and hyperbolic functions, were determined from the boundary conditions in terms of the maximum shear stress. The lateral normal stress was then given in terms of an "effective" tension modulus of the adhesive, whose value is difficult to establish theoretically. The conclusions drawn by Hart-Smith on the stress distributions are

1) The highest shear stress in the adhesive was at the end of overlap near the leading end of the less stiff adherend.

2) For long overlaps, the magnitude of the maximum shear stress did not vary with length; only the stress in the central portion of the joint was lowered by increasing length.

3) Lateral normal stresses were reduced by using a thin outer adherend, or an adherend with a low extensional modulus, or a thick adhesive layer. Thus, the lateral normal stresses can be reduced at the expense of the shear stresses.

4) The characteristic extent of the end zones was independent of the length of overlap.

2.3 Finite Element Studies

2.3.1 Introduction

The use of finite element methods of analysis means, in principle, that the simplifying assumptions made in the classical analytical methods need not be made. The technique does allow the solution of problems that are totally intractable by classical methods. Basically, one can choose between a large number of primitive elements, i.e., elements in which strain is assumed to be constant, or a smaller number of more sophisticated elements, ones with linear or quadratic strain variation. Whatever idealization is adopted, a higher

density (finer mesh) of elements is necessary in regions of rapidly varying stress.

Finite element analysis of an adhesive-bonded joint was first performed in 1969. Considerable work has been done with finite element analysis of adhesive-bonded joints of fiber reinforced composite materials.

2.3.2 Ahluwalia's Analysis

The first finite element analysis of an adhesive bonded joint was made by Ahluwalia [9]. He analyzed a double-lap joint. The finite element solution for the double lap joint was for plane strain with 120 nodal points and 188 triangular elements. The adhesive was divided into ten equal elements along its length and was made of one element across the thickness. Consequently, the high magnitude of the stresses at and near the ends of the overlap were not correctly determined, and the stresses did not vary across the thickness of the adhesive. Smaller elements were not defined at the ends of the overlap where shear and lateral normal stress concentrations exist. The shear and lateral normal stress distributions were nonuniform with peaks at the ends of the overlap. Large sizes of elements in areas of very sharply rising peak stresses result in lower magnitude of the calculated stresses.

2.3.3 Wooley and Carver's Analysis

Wooley and Carver [10] analyzed a single lap adhesive-bonded joint with the finite element method. The finite element solution for the single lap adhesive-bonded joint was for plane stress problem with 497 nodal points and 394 elements.

The solution was based on the computer program "ARBAS" by E.L. Wilson of the University of California at Berkeley. The locating of nodal points was accomplished by dividing the configuration into three parts, the section of the lap joints, and the sections to each side of the lap. In the program, quadrilateral elements, composed of four triangular elements, were used to describe the joint. The displacements of the triangular elements were described by linear functions which resulted in a constant strain and, therefore, constant stress over each element.

The adhesive layer was divided into two equal elements through its thickness and twenty equal elements along its length. The maximum aspect ratio of a quadrilateral element in the adhesive was 100:1. The single-lap adhesive-bonded joint was made of identical adherends with an elastic adhesive. The Poisson's ratios of the adhesive and adherends were 0.3 for all the cases. The range of the ratio of the elastic moduli of the adherend and adhesive, E/E_a was from 0.1 to 1000. The range of the ratio of the thickness of the adhesive and adherends, t_a/t was from 0.02 to 0.1. The length

of overlap was taken as 5, 10 and 20 times the adherend thickness.

The stress distributions at the adhesive-adherend interface were not given. The stress distributions at the mid plane of the adhesive layer were nonuniform with peaks near the ends of the overlap for both shear and lateral normal stresses. They compared the stress concentrations obtained by each method at three values of the geometric and material parameters. With two elements across the adhesive thickness, the variation of the stresses across the adhesive thickness can not be adequately represented.

2.4 Experimental Studies

2.4.1 Mclaren and MacInnes's Investigation

Mclaren and MacInnes [11] conducted photoelasticity experiments on single lap joints. The object of their investigation was to verify the mathematical analysis of Goland and Reissner. Two series of tests were performed. In the first series, the complete joint was made of Araldite. In the second series of tests, the adherends were made of aluminum and the adhesive of Araldite. The ratio of the modulus of the adhesive to that of the adherend was 1/20 in the second series of tests. The results were presented in terms of the fringe order, and no attempt was made to determine the magnitude of the stresses. The difference between these two model systems was in the transfer of load

from one adherend to the other. The adhesive in the second series was in longitudinal shear across its entire thickness; thus, the transfer of load was primarily by shear. Their investigation supports the theory of Goland and Reissner in that the qualitative aspects of the theory are well corroborated.

2.4.2 Tuzi and Shimada's Investigation

Tuzi and Shimada [12] conducted a photoelastic investigation of a single lap joint. Their investigation concentrated mainly on stress concentration in the joint. Single lap joint models having different adhesive shapes at the ends of overlap; rectangular type, with a fillet and with convex and concave semi-circular ends were used in the photoelastic investigation.

The adhesive layer of the joint was made of epoxy rubber and the adherends were represented by epoxy resin and duralumin. In the first experiment, the adherends were made of epoxy resin KT-102 and the adhesive layer was made of an epoxy rubber. The adhesive was bonded to the adherends by Araldite D. In the second experiment, the adherends were made of duralumin, the adhesive layer was made of epoxy resin KT-102, and the adhesive was bonded to the adherends by Araldite D. Their experimental results indicated that the joint with concave semicircular ends was the best, the one with rectangular ends was second best, and the one with convex

semicircular ends was the worst as regards the stress concentration in the joint. They also studied the stress distributions in scarf and butt joints photoelastically. Their photoelastic models were made of epoxy resin and epoxy rubber and also epoxy resin and metal. Tension and bending tests were carried out on bars bonded at various angles. For the joints with a soft adhesive layer bonded to hard adherends, the stress concentrations were maximum at the ends of the bonded boundary with an obtuse angle. For the joints with a hard adhesive layer bonded to soft adherends, the stress concentrations were found at the ends of the bonded boundary with an acute angle.

CHAPTER 3
LINEAR ELASTIC STRESS ANALYSIS

3.1 Introduction

The joint under consideration is a double-doubler joint (Figure 3.1). This joint is subjected to two different loading cases (constant tensile loading and pure bending). In this chapter the three materials (central adherend, adhesive, outer adherend) are assumed to behave in a linear elastic manner under the applied loads. The elastic properties, Young's modulus and the Poisson's ratio are E_c and ν_c for central adherend; E_a and ν_a for the adhesive layer; E_o and ν_o for the outer adherend. The material properties are extended to orthotropic material properties for the application to composite adherends.

The overall problem is to find the stress distributions in the double-doubler adhesive bonded joint under the applied load. The distributions along the axial direction of the stresses on the interface between the central adherend and adhesive, and of the cohesive stresses at various levels in the adhesive are the particular interest in this study. The analysis can be simplified to either a plane stress or a plane strain problem. For most practical purposes the width of an adhesive joint is large compared to the thickness of the

adherend and the adhesive. Therefore the plane strain analysis option is used throughout. First of all linear elastic stress analysis for double-doubler reinforcement of a continuous member (Figure 3.1a) was carried out. The results, are compared with the previous experimental results and they show good agreement. After that the linear elastic stress analysis for a double-doubler joint (Figure 3.1b) was investigated. The finite element method of stress analysis is applied to this plane problem involving different materials. The reason why the finite element method is chosen over any other method is that geometrically complex bodies of different materials can be easily represented and arbitrary distributions of displacement and stress boundary conditions can be specified.

For this linear elastic stress analysis the finite element program ANSYS is employed in the finite element studies of the double-doubler joint.

3.2 Joint Description

The geometry and dimension of the joint are shown in Figure 3.2. The basic material properties used in this joint are given in Table 3.1.

outer adherend

central adherend

y

adhesive

x

a) the double-doubler reinforcement
of a continous member

outer adherend

central adherend

y

adhesive

x
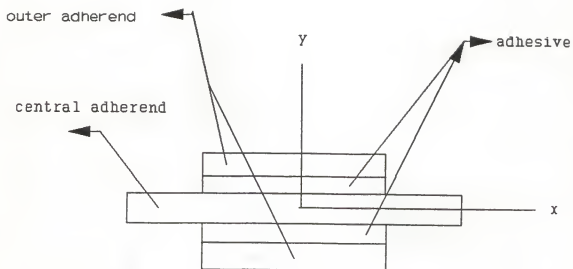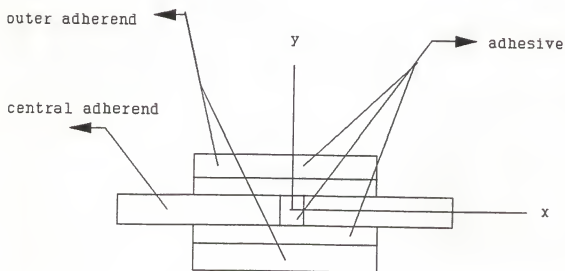
b) the double-doubler joint

Figure 3.1 Double-doubler joint configuration
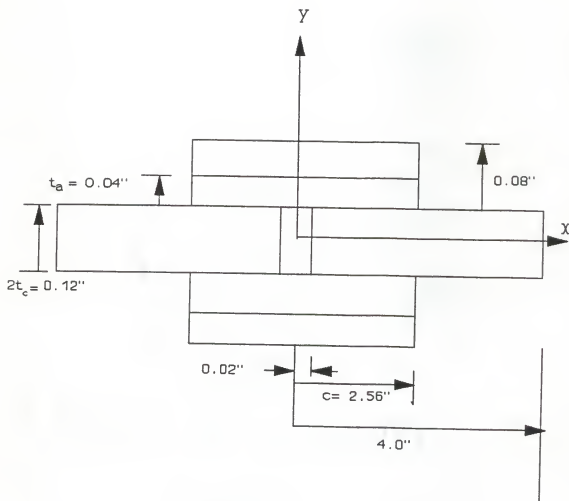
Figure 3.2 Double-doubler joint geometry

Table 3.1. Elastic Material Properties Used in Analysis

Mateial	Modulus,E	Poisson's ratio	Shear Modulus,G
aluminum	10.6E6 psi	0.33	
epoxy	3.6E6 psi	0.39	
graphite epoxy	22.8E6[a] psi 1.58E6[b] psi	0.3[c]	0.81E6[d] psi

a: Longitudinal modulus of unidirectional composite i.e. fiber direction
b: Transverse modulus of composite
c: Major Poisson's ratio of unidirectional composite
d: Inplane shear modulus

3.3 Determining Material Properties

The strain-stress relations for anisotropic materials can be expressed as

$$\epsilon_i = s_{ij}\ \sigma_j \qquad i,j = 1,2,-----,6 \qquad 3.1$$

where ϵ_i are the strain components, s_{ij} are the elements of the compliance matrix, and σ_j are the stress components. Equation 3.2 gives the form of the relations for a unidirectional fiber reinforced lamina with axes x_1, x_2, x_3 aligned with the principal material directions as shown in Figure 3.3. (x_1 corresponds to fiber direction, x_2 is the in-plane coordinate perpendicular to x_1, and x_3 is the tranverse coordinate which is perpendicular to the x_1-x_2 plane.)

$$
\begin{bmatrix} \epsilon_1 \\ \epsilon_2 \\ \epsilon_3 \\ \epsilon_4 \\ \epsilon_5 \\ \epsilon_6 \end{bmatrix}
=
\begin{bmatrix}
S_{11} & S_{12} & S_{13} & 0 & 0 & 0 \\
S_{12} & S_{22} & S_{23} & 0 & 0 & 0 \\
S_{13} & S_{23} & S_{33} & 0 & 0 & 0 \\
0 & 0 & 0 & S_{44} & 0 & 0 \\
0 & 0 & 0 & 0 & S_{55} & 0 \\
0 & 0 & 0 & 0 & 0 & S_{66}
\end{bmatrix}
\begin{bmatrix} \sigma_1 \\ \sigma_2 \\ \sigma_3 \\ \sigma_4 \\ \sigma_5 \\ \sigma_6 \end{bmatrix}
\qquad 3.2
$$
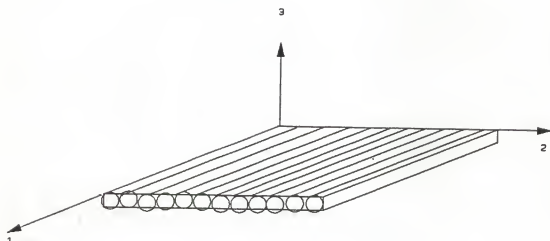
Figure 3.3 Material principal coordinate system

The compliances can be expressed in terms of engineering constants as follows:

$$S_{11} = 1/E_{11} \qquad S_{12} = -\nu_{12}/E_{11} \qquad S_{13} = -\nu_{13}/E_{11}$$
$$S_{22} = 1/E_{22} \qquad S_{23} = -\nu_{23}/E_{22} \qquad S_{33} = 1/E_{33} \qquad 3.3$$
$$S_{44} = 1/G_{12} \qquad S_{55} = 1/G_{23} \qquad S_{66} = 1/G_{13}$$

where

E_{11}, E_{22}, E_{33} are Young's moduli in 1,2 and 3 directions respectively.

ν_{ij} is Poisson's ratio determined from contraction in the x_j direction during a tensile test in the x_i direction

G_{ij} is shear moduli in the x_i-x_j planes

We know that the following relationships exist between the Young's moduli and the Poisson's ratios due to symmetry of the compliance

$$E_{11}\nu_{21} = E_{22}\nu_{12}, \quad E_{22}\nu_{32} = E_{33}\nu_{23}, \quad E_{33}\nu_{13} = E_{11}\nu_{31} \qquad 3.4$$

Thus for an orthotropic material, constitutive relations are

$$
\begin{bmatrix} \epsilon_1 \\ \epsilon_2 \\ \epsilon_3 \\ \epsilon_4 \\ \epsilon_5 \\ \epsilon_6 \end{bmatrix}
=
\begin{bmatrix}
1/E_{11} & -\nu_{12}/E_{11} & -\nu_{13}/E_{11} & 0 & 0 & 0 \\
-\nu_{12}/E_{11} & 1/E_{22} & -\nu_{23}/E_{22} & 0 & 0 & 0 \\
-\nu_{13}/E_{11} & -\nu_{23}/E_{22} & 1/E_{33} & 0 & 0 & 0 \\
0 & 0 & 0 & 1/G_{12} & 0 & 0 \\
0 & 0 & 0 & 0 & 1/G_{23} & 0 \\
0 & 0 & 0 & 0 & 0 & 1/G_{13}
\end{bmatrix}
\begin{bmatrix} \sigma_1 \\ \sigma_2 \\ \sigma_3 \\ \sigma_4 \\ \sigma_5 \\ \sigma_6 \end{bmatrix}
$$

3.5

For a transversely isotropic material in which the x_2-x_3 plane is the plane of isotropy, we find $E_{22} = E_{33}$, $G_{13} = G_{12}$, $\nu_{12} = \nu_{13}$ and $G_{23} = E_{22}/2(1+\nu_{23})$. If we invert Equation 3.5, for a material having tranverse isotropy relative to the $x_2 - x_3$ plane, we obtain the elastic stiffness, C_{ij}, in terms of engineering constants with the following results:

$$C_{11} = (1 - \nu^2{}_{23})\ E_{11}/V$$

$$C_{13} = C_{12} = \nu_{12}(1 + \nu_{23})\ E_{22}/V$$

$$C_{23} = (\nu_{23} + \nu^2{}_{12}E_{22}/E_{11})\ E_{22}/V$$

$$C_{33} = C_{22} = (1 - \nu^2{}_{12}E_{22}/E_{11})\ E_{22}/V \qquad\qquad 3.6$$

$$C_{44} = G_{23} = E_{22}/2(1 + \nu_{23})$$

$$C_{55} = C_{66} = G_{12}$$

where $V = [(1 + \nu_{23})(1 - \nu_{23} - 2\nu^2{}_{12}E_{22}/E_{11})]$

For the plane strain case, E_{11}, E_{22}, E_{33}, ν_{12}, ν_{13}, ν_{23}, G_{12}, G_{13}, G_{23} would be used as input data for ANSYS. If G_{12}, G_{13}, G_{23} are not specified, they are computed as:

$$G_{12} = E_1E_2/(E_1 + E_2 + 2\nu_{21}E_1)$$

$$G_{23} = E_2E_3/(E_2 + E_3 + 2\nu_{32}E_2) \qquad\qquad 3.7$$

$$G_{13} = E_1E_3/(E_1 + E_3 + 2\nu_{13}E_1)$$

3.4 Finite Element Model Representation

Only one quarter of the model is selected for analysis of the simple tension loading case, because it has double symmetry in geometry, materials, boundary, and loading conditions. One half of the model is chosen for the pure bending loading case.

The ANSYS two-dimensional isoparametric element which accomodates orthotropic material properties is used. The element is defined by four nodal points, each having two degree of freedom. The plane strain option is used. The displacement boundary conditions imposed on simple tension and pure bending case are shown in Figure 3.4. In simple tension cases analyzed in this study, the double-doubler joint is subjected to 50 lb at the outer end of the central adherend. In pure bending case, a linear varying force boundary condition equivalent to a couple is used at the outer end of the central adherend. For the input of the orthotropic material properties the classical thin plate lamination theory is used to calculate the effective material properties for the laminate. For unidirectional composite lamina, properties in the thickness direction are calculated assuming that $E_{22} = E_{33}$, $\nu_{12} = \nu_{13}$ and $\nu_{23} =$ matrix Poisson's ratio.

The material principal coordinate system (1,2,3) refers to the fiber and two transverse matrix directions, respectively. (See Figure 3.3) The computer program can be used to calculate effective material properties for composite laminates. The mesh is so generated that around the bonding corner and on the boundary between two different materials the grids are much finer than those of other locations for better results in these regions of high stress gradients. The finite element dimensions which are used in the analysis for the high stress concentration regions are shown in Figure 3.5.

a) imposed boundary condition on simple tension loading

b) imposed boundary condition on pure bending
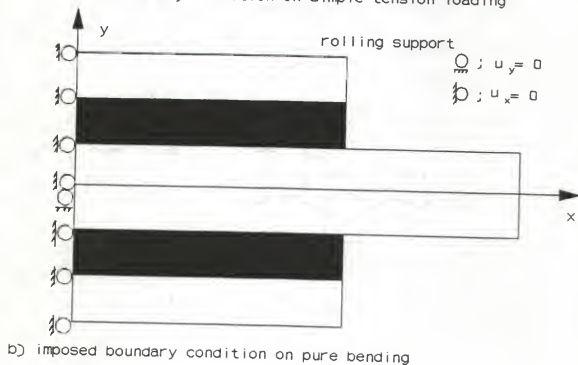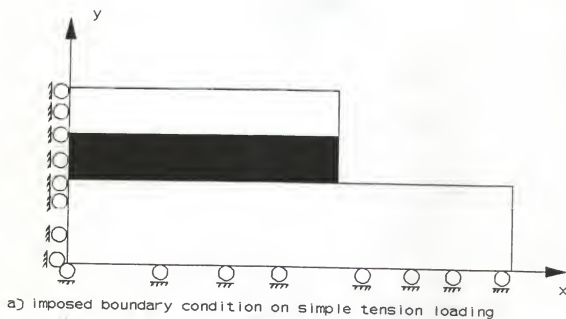
Figure 3.4 Displacement boundary conditions for
simple tension and pure bending
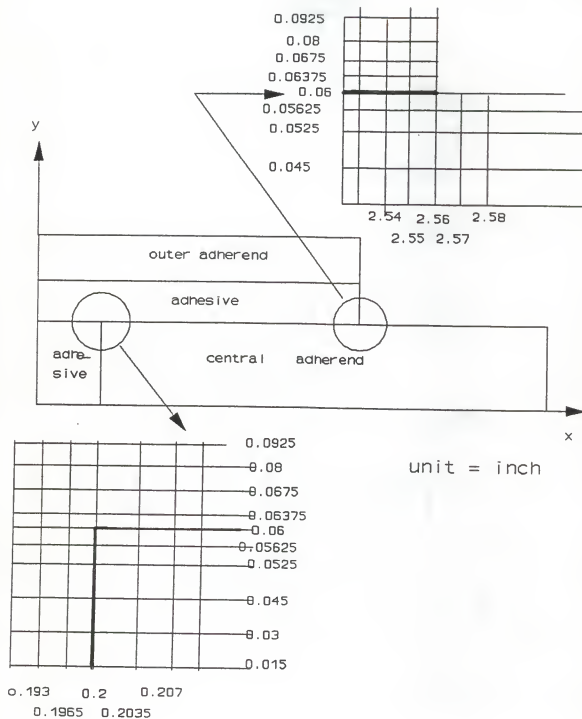
Figure 3.5 The finite element mesh coordinates for the high stress concentration regions

A total of 1591 nodes and 1456 elements for the simple tension case, and 2819 nodes and 2672 elements for the pure bending case are used. (See Figure 3.6 and Figure 3.7) The numbers in circles relate to the nodal-point numbers. Those within the mesh relate to element numbers. The model is constructed using ANSYS STIF42.

3.5. Finite Element Results

In all the stress distribution results, the stresses are normalized with respect to the average applied axial stress, p_{av}, acting on the central adherend. Accordingly $\underline{\sigma}_x = \sigma_x/p_{av}$, $\underline{\sigma}_y = \sigma_y/p_{av}$, $\underline{\sigma}_{xy} = \sigma_{xy}/p_{av}$, while $\underline{x} = x/c$.

where σ_x: axial normal stress

σ_y: lateral normal stress

σ_{xy}: shear stress

p_{av}: applied average stress

c: 2.56 inches

For nodal stress, the stresses at each node are computed by averaging the nodal stresses of the node being processed for all elements that are connected to that node. In other words, the component nodal stresses that are automatically stored per element are averaged at a node whenever two or more elements connect to the same node. For example average nodal stress σ_x at the node N can be calculated as below.
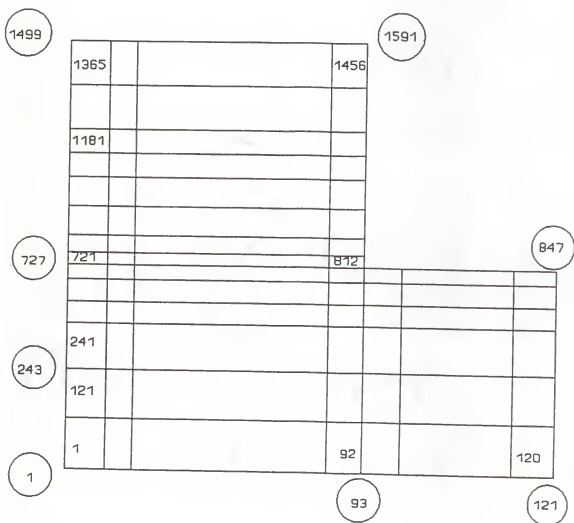
Figure 3.6 The layout of finite element mesh in simple tension
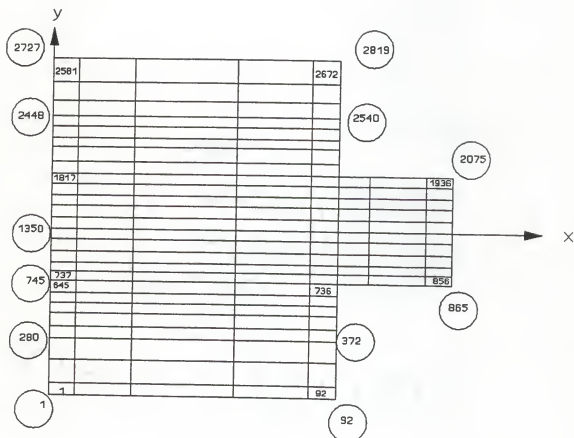
Figure 3.7 The layout of finite element mesh in pure bending

element1	
element2	element3

From element 1 σ_x at node N
From element 2 σ_x at node N
From element 3 σ_x at node N

$$\text{average nodal stress} = (\sigma_{1x} + \sigma_{2x} + \sigma_{3x})/3$$

Four cases are considered in the following four subsections. Case 1 and 2 are for two different choices of adherends with simple tension loading. Case 3 and 4 are for the same two choices of adherends as case 1 and 2, but with pure bending loading. Each of the four cases is treated first for double-doubler reinforcement of a continuous member, and then for a double-doubler lap joint.

3.5.1 Case 1. Aluminum Adherends and Epoxy Adhesive in Simple Tension

The model for the first case is composed of aluminum adherends and an epoxy adhesive. For double-doubler reinforcement of a continuous member (Figure 3.1a), the axial distribution of the lateral normal stress (σ_y), and the shear stress (σ_{xy}) along the boundary between central adherend and adhesive are plotted from the averaged nodal stress values. The reason why the averaged nodal stress values are used is that the lateral normal (σ_y) and shear stress (σ_{xy}) are continous across the interface. These stress distributions are shown in Figure 3.8. From these graphs and the known symmetry about the mid-length, we can see that the stress distributions (σ_y, σ_{xy}) along the axial direction are very

Figure 3.8 Case 1. The stress distributions of double-doubler
reinforcement of a continous member along the
boundary between the central adherend and adhesive

uniform and at a very low level for -0.75< x/c <0.75. But near the free edges (for 0.75 < x/c < 1 and -1 < x/c <-0.75) we can see sharp variation of stresses and see the peak stresses at the free end of adhesive. Different peak stress values are obtained depending upon the size of the mesh element. This means that calculated stress fields near this area are not quite reliable.

In linear elastic analysis, stress fields near the two bonding edges show singular behavior. In order to describe the stress fields near these corners, singular stress parameters are used in Chapter 5.

The cohesive stress distributions along the axial direction at different levels of y of the adhesive were obtained. These different levels of y in the adhesive strip is shown in Figure 3.9. According to the results which are shown in Appendix A, the axial distribution of shear stress (σ_{xy}) at the level of y=0.06375 shows a similar trend to that in the stress distribution along the boundary between central adherend and adhesive. The axial distribution of axial normal stress (σ_x) at the same level of y=0.06375 shows a similar trend as that in the stress distribution along the boundary between central adherend and adhesive, except that the axial normal stress distribution drops toward zero near the free end of the adhesive layer. The axial distribution of lateral normal stress (σ_y) near the free end shows a similar trend to that in the stress distribution along the boundary between
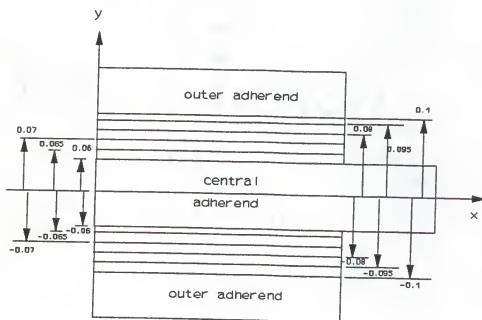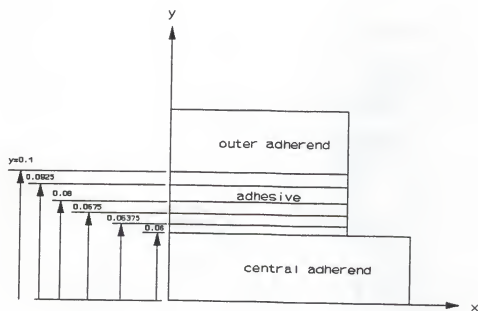
Figure 3.9 The different levels of y in the adhesive strip

central adherend and adhesive, except that the peak stress value becomes lower than previous peak stress on the boundary.

The axial distribution of axial normal stress (σ_x) and lateral normal stress (σ_y) at the higher level (y=0.0675) than the previous case (y=0.06375) shows a similar trend, except that the peak stress values are lower than ones of the previous case. The axial distribution of shear stress (σ_{xy}) near the free end zone, which is taken from the level of y=0.0675, rises steeply, far beyond its average level, and drops steeply near the free end to near zero. These stress distribution trends are similar to the case which is taken from the upper level of the adhesive at y=0.08. The stress distribution at the level of y=0.0925 shows same trend as the previous case except that the lateral normal stress (σ_y) changes its sign and drops to a negative value which means compressive stress, immediately after the peak positive value in the end zone.

The axial distributions of stresses (σ_y, σ_{xy}) along the boundary between adhesive and outer adherend are plotted in the same way as for the boundary between the central adherend and adhesive. The results are shown in Figure 3.10. They show that the shear stress (σ_{xy}) drops to near zero near the free end. The lateral normal stress (σ_y) shows that after the peak positive stress value near the end zone, it suddenly drops to the negative value which means compressive stress.

We find that along the boundary between the central or

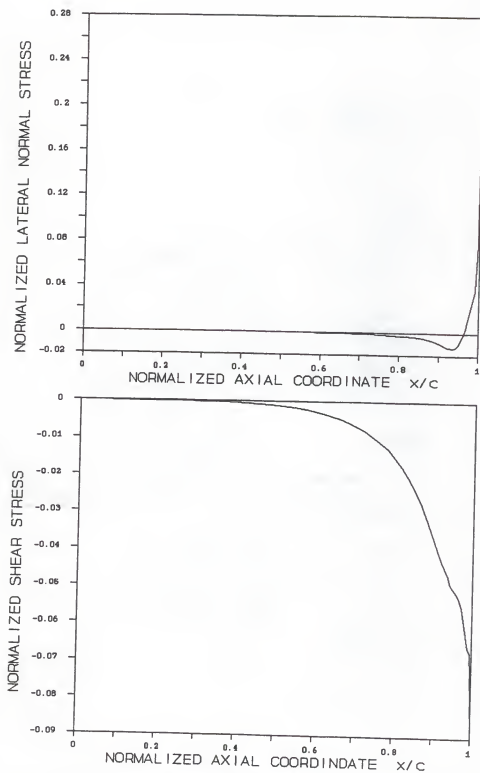Figure 3.10 Case 1. The stress distributions of double-doubler
reinforcement of a continous member along the
boundary between the outer adherend and adhesive

outer adherend and adhesive the stress is not well defined at the ends of adhesive. Therefore one would not expect the free end condition ($\sigma_x=0$, $\sigma_{xy}=0$) to be satisfied at the very near end zone. However, the end condition ($\sigma_{xy}=\sigma_x=0$) at the various levels inside the adhesive, which means no external traction force in the x or y direction, is almost satisfied even by using the displacement finite element method .

To check the stress variation through the thickness direction of the adhesive, the interlaminar adhesive layer is divided into four longitudinal strips as shown in Figure 3.9. The results from the data plotted for various levels of y in Appendix A show that through the adhesive thickness the shear, axial and lateral normal stresses are pretty uniform through the adhesive thickness within the zone $-0.975 < x/c < 0.975$, but near the free end zones ($0.98 < x/c < 1$ and $-1 < x/c < -0.98$) the stress changes rapidly through the adhesive thickness. If we assume that the stresses are uniform through the adhesive thickness, we can not predict the compressive lateral normal stress of the adhesive layer.

For a double-doubler lap joint (Figure 3.1b), the stress distributions on the boundaries between central adherend and adhesive and between outer adherend and adhesive are shown in Figure 3.11 and Figure 3.12, respectively. The axial distributions of stress at different levels of y are shown in Appendix B. From the results we find that the axial distribution of the lateral normal stress (σ_y), axial normal

Figure 3.11 Case 1. The stress distributions of a double-
doubler joint along the boundary between
the central adherend and adhesive

Figure 3.12 Case 1. The stress distributions of a double-doubler joint along the boundary between the outer adherend and adhesive

stress (σ_x) and the shear stress (σ_{xy}) are very uniform and at a very low level between 0.3 < x/c <0.8 and −0.3 < x/c <−0.8. But near the corner edge of adhesive line and bonded corner at the butted region between two central adherends, there is a very high stress concentration and very complicated stress distribution. The peak stress values obtained from the finite element method are not quite reliable, since the peak values vary depending upon the mesh size. The stress distributions, except near the bonded corner in the butted region, show similiar trends to the ones of double-doubler reinforcement of a continous member. Near the bonded corner of the butted region, the shear stress (σ_{xy}) is very large. The lateral normal stress (σ_y) has its highest peak value at the edge of the interface between central adherend and adhesive. This lateral normal stress (σ_y) becomes compressive at the level of y=0.0925 which is very near the interface between adhesive and outer adherend, and at that interface it shows very high compressive lateral normal stress (σ_y).

3.5.2 Case 2. Aluminum Central Adherend, Epoxy Adhesive, and Composite Outer Adherend in Simple Tension

The model for the second case is composed of aluminum central adherend, epoxy adhesive and graphite/epoxy composite outer adherend. A unidirectional graphite/epoxy laminate is used for outer adherend.

For double-doubler reinforcement of a continous member, the axial distribution of the cohesive lateral normal stress(σ_y), shear stress(σ_{xy}) and the axial normal stress(σ_x) are plotted from the averaged nodal stress values and are shown in Appendix C for various levels of y. The axial distribution of the lateral normal stress and shear stress along the boundary between the central adherend and adhesive are plotted from the averaged nodal stress values stress and are shown in Figure 3.13. The stress distributions on the boundary between the adhesive and outer adherend are plotted in the same way and are shown in Figure 3.14.

For a double-doubler joint, the axial distributions of the cohesive stress at different levels of y are plotted and shown in Appendix D. The stress distributions on the boundary between the central adherend and adhesive, and the outer adherend and adhesive, are shown in Figure 3.15 and Figure 3.16, respectively. The stress distribution trends are similar to Case 1, but higher peak stress values are obtained from Case 2.

3.5.3 Case 3. Aluminum Adherends and Epoxy Adhesive in Pure Bending

The model for Case 3 is composed of aluminum adherends and epoxy adhesive and is under pure bending in the positive sense (concave upward). A linear varying force boundary
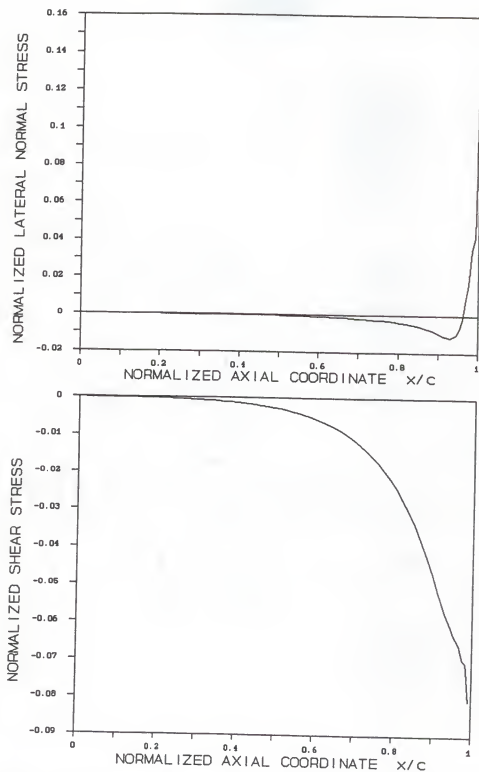
Figure 3.13 Case 2. The stress distributions of double-doubler
reinforcement of a continous member along the
boundary between the central adherend and adhesive

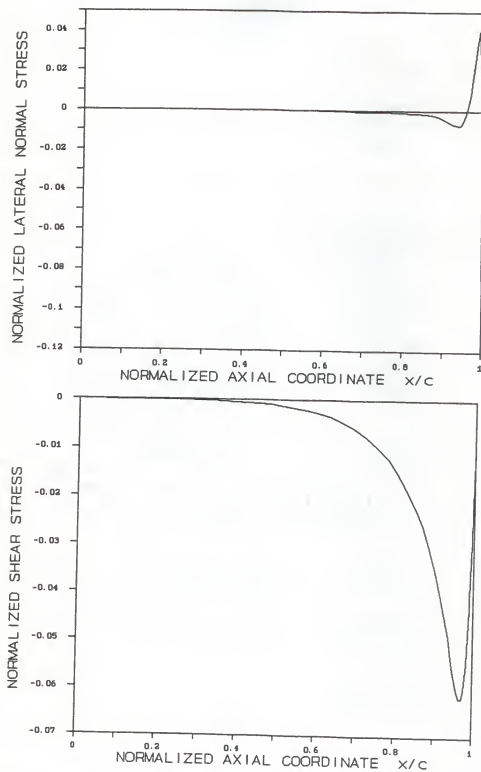Figure 3.14 Case 2. The stress distributions of double-doubler
reinforcement of a continous member along the
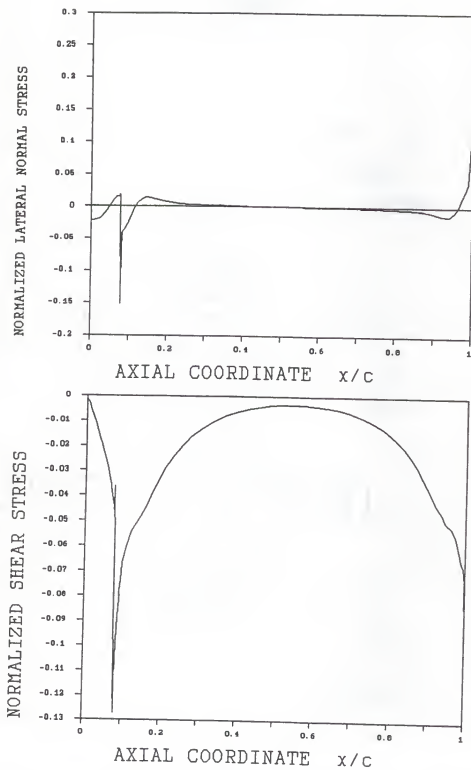boundary between the outer adherend and adhesive

Figure 3.15 Case 2. The stress distributions of a double-
doubler joint along the boundary between
the central adherend and adhesive
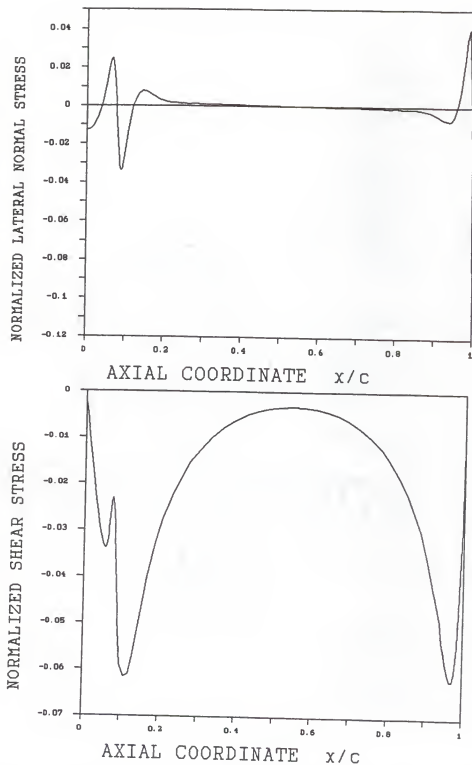
Figure 3.16 Case 2. The stress distributions of a double-doubler joint along the boundary between the outer adherend and adhesive

condition equivalent to a couple is used at the outer end of the central adherend.

For double-doubler reinforcement of a continous member, the axial distributions of the cohesive stress are plotted from the averaged nodal stress values and shown in Appendix E. We have four overlap interfaces in the pure bending case. The axial stress (σ_y, σ_{xy}) distributions on the boundaries between the central adherend and upper adhesive and between the upper outer adherend and adhesive are plotted from averaged nodal stress values and shown in Figure 3.17 and Figure 3.18, respectively. The axial stress distributions (σ_y, σ_{xy}) on the boundaries between the central adherend and lower adhesive and between the lower outer adherend and adhesive are shown in Figure 3.19 and Figure 3.20, respectively. As expected, the shear stress is symmetric with respect to the mid plane, while the lateral normal stress is approximately antisymmetric.

For a double-doubler lap joint, the axial distributions of the cohesive stress for various levels of y in the upper and lower adhesive are shown in Appendix F. The axial stress distributions (σ_y, σ_{xy}) on the boundary between the central adherend and upper adhesive and between the upper outer adherend and adhesive are shown in Figure 3.21 and Figure 3.22, respectively. The axial stress distributions (σ_y, σ_{xy}) on the boundary between the central adherend and lower

adhesive and between the lower outer adherend and adhesive are shown in Figure 3.23 and Figure 3.24, respectively.

Figure 3.17 Case 3. The stress distributions of double-doubler
reinforcement of a continous member along the
boundary between the central adherend and upper
adhesive

Figure 3.18 Case 3. The stress distributions of double-doubler reinforcement of a continous member along the boundary between the upper outer adherend and adhesive

Figure 3.19 Case 3. The stress distributions of double-doubler
reinforcement of a continous member along the
boundary between the central adherend and lower
adhesive

Figure 3.20 Case 3. The stress distributions of double-doubler of a continous member along the boundary between the lower outer adherend and adhesive

Figure 3.21 Case 3. The stress distributions of a double-doubler joint along the boundary between the central adherend and upper adhesive

Figure 3.22 Case 3. The stress distributions of a double-doubler joint along the boundary between the upper outer adherend and adhesive
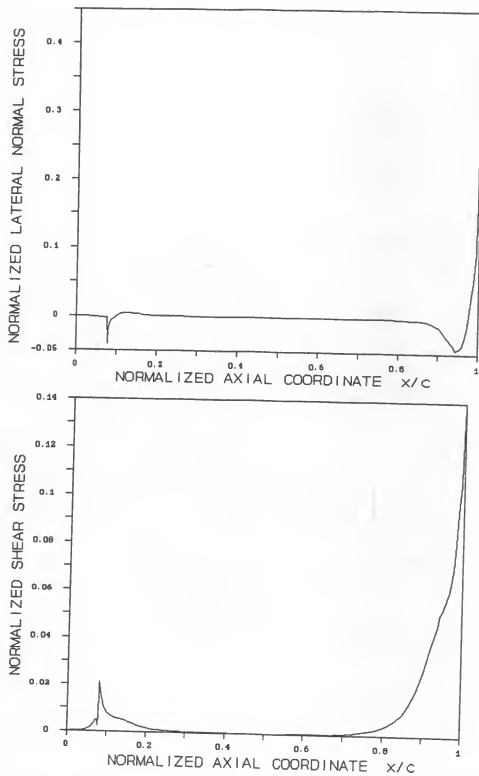
Figure 3.23 Case 3. The stress distributions of a double-doubler joint along the boundary between the central adherend and lower adhesive
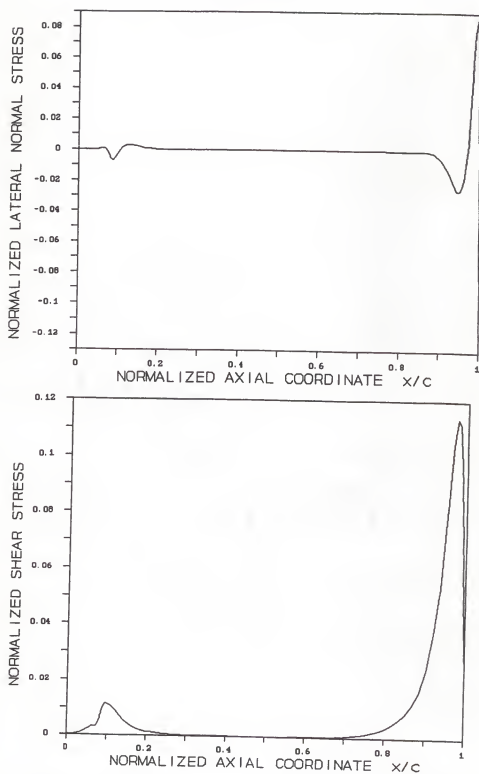
Figure 3.24 Case 3. The stress distributions of a double-doubler joint along the boundary between the lower outer adherend and adhesive

3.5.4 Case 4. Aluminum Central Adherend, Epoxy Adhesive, and Composite Outer Adherend in Pure Bending

The model for Case 4 consists of aluminum central adherend, epoxy adhesive, and graphite/epoxy outer adherend under pure bending in the positive sense.

For double-doubler reinforcement of a continous member, the axial distributions of the cohesive stress at various levels of y in the upper adhesive are shown in Appendix G. The axial stress distributions (σ_y, σ_{xy}) on the boundary between the central adherend and upper adhesive and between the upper outer adherend and adhesive are shown in Figure 3.25 and Figure 3.26, respectively. The axial stress distributions (σ_y, σ_{xy}) on the boundary between the central adherend and lower adhesive and between the lower outer adherend and adhesive are shown in Figure 3.27 and Figure 3.28, respectively.

For a double-doubler lap joint, the axial distributions of the cohesive stresses for various levels of y in the upper adhesive are shown in Appendix H. The stress distributions (σ_y, σ_{xy}) on the boundary between the central adherend and upper adhesive and between the upper outer adherend and adhesive are shown in Figure 3.29 and Figure 3.30, respectively. The stress distributions (σ_y, σ_{xy}) on the boundary between the central adherend and lower adhesive and between the lower outer adherend and adhesive are shown in Figure 3.31 and Figure 3.32, respectively. The stress

distribution trends are similar to Case 3, but higher peak stress values are obtained from Case 4.
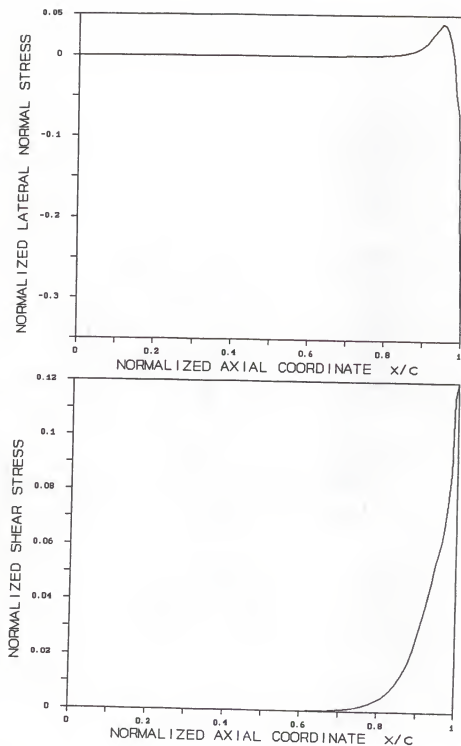
Figure 3.25 Case 4. The stress distributions of double-doubler reinforcement of a continous member along the boundary between the central adherend and upper adhesive
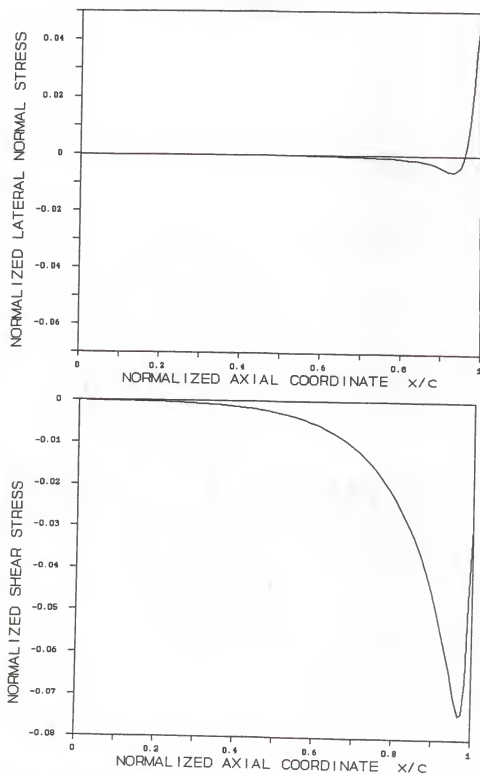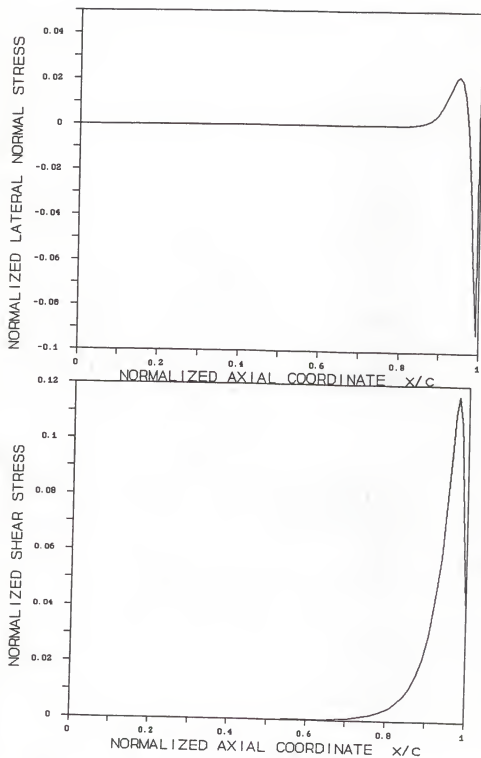
Figure 3.26 Case 4. The stress distributions of double-doubler
reinforcement of a continous member along the
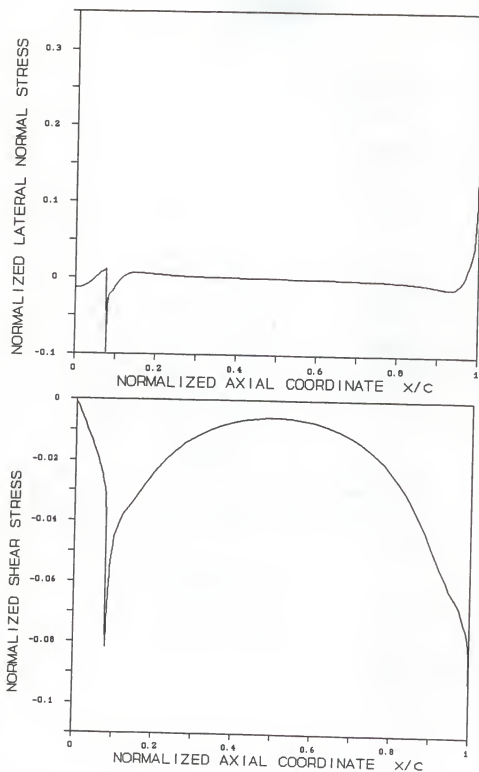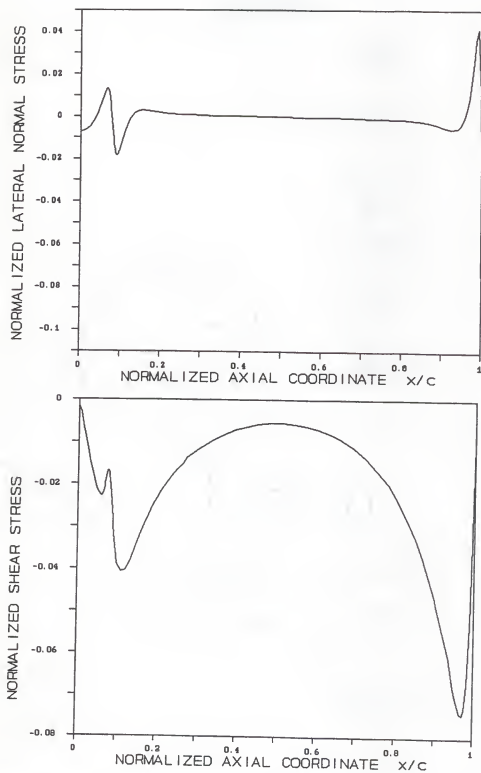boundary between the upper outer adherend and
adhesive
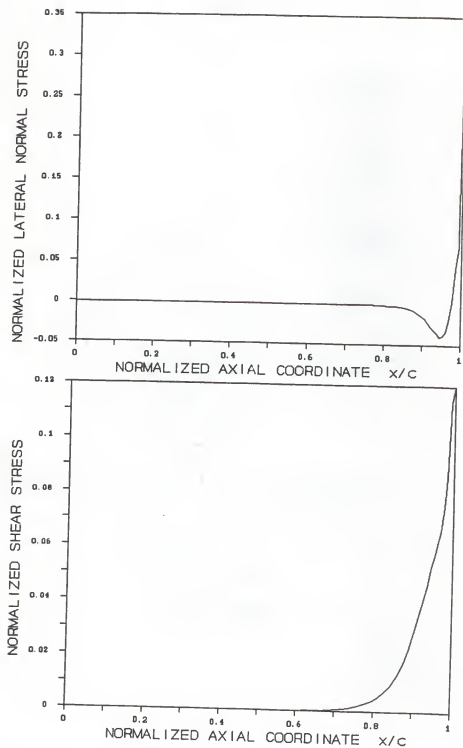
Figure 3.27 Case 4. The stress distributions of double-doubler reinforcement of a continuous member along the boundary between the central adherend and lower adhesive
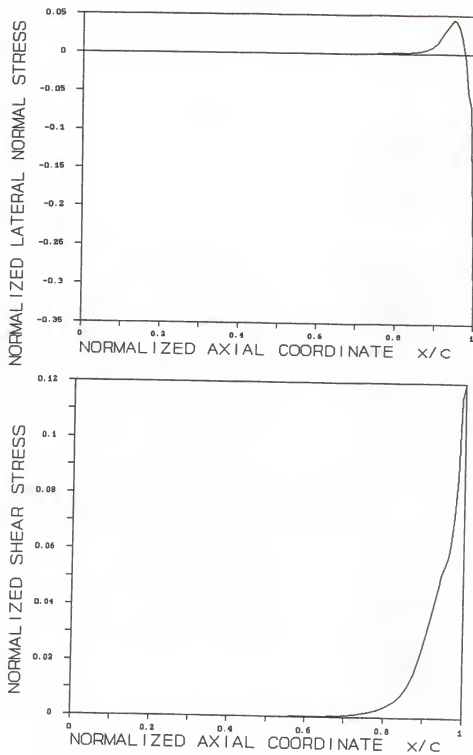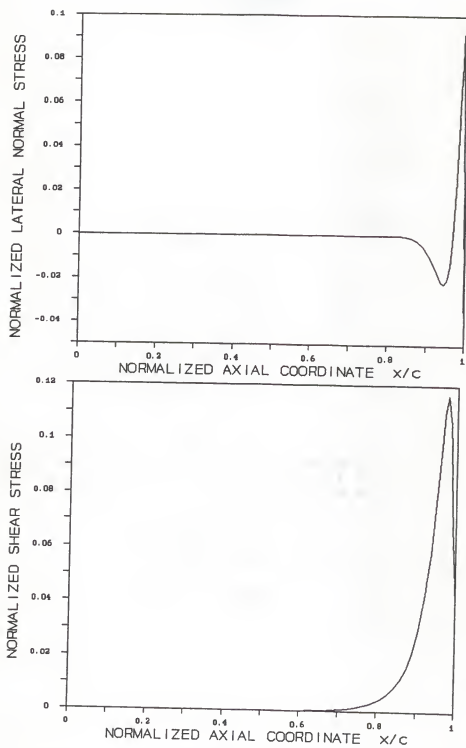
Figure 3.28 Case 4. The stress distributions of double-doubler
reinforcement of a continous member along the
boundary between the lower outer adherend and
adhesive
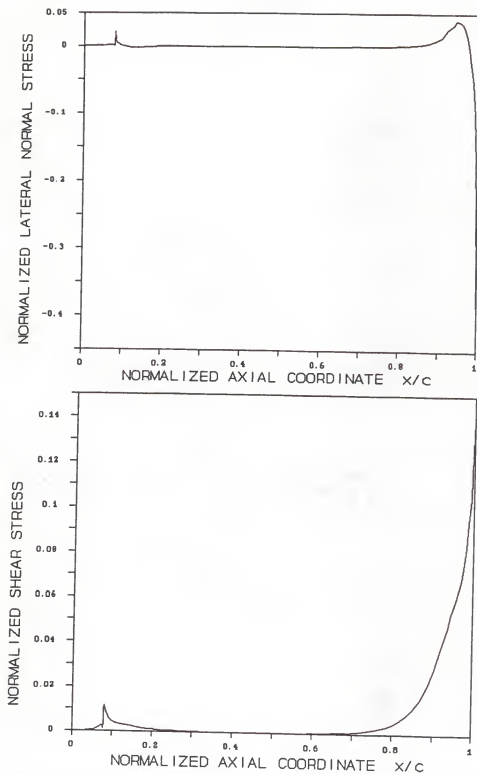
Figure 3.29 Case 4. The stress distributions of a double-doubler joint along the boundary between the central adherend and upper adhesive
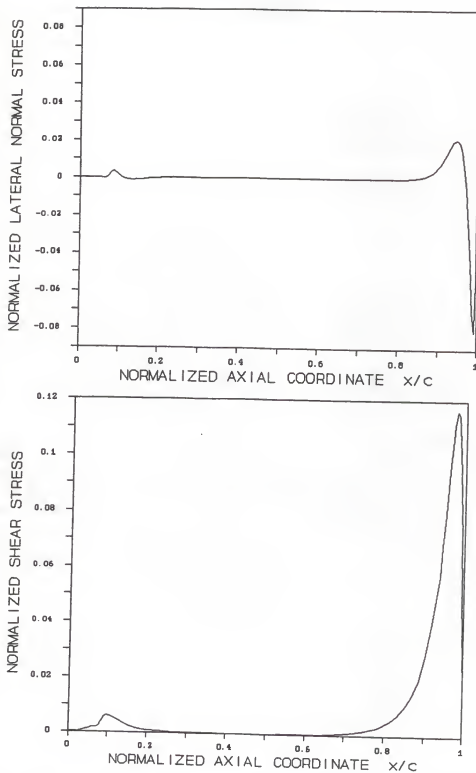
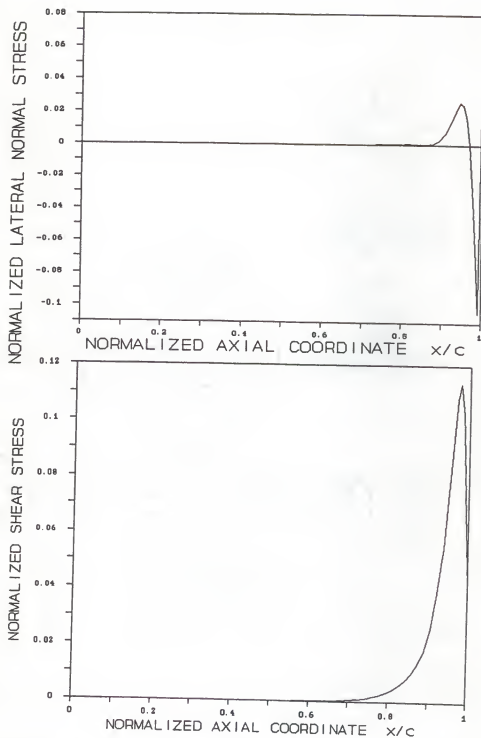Figure 3.30 Case 4. The stress distributions of a double-doubler joint along the boundary between the upper outer adherend and adhesive
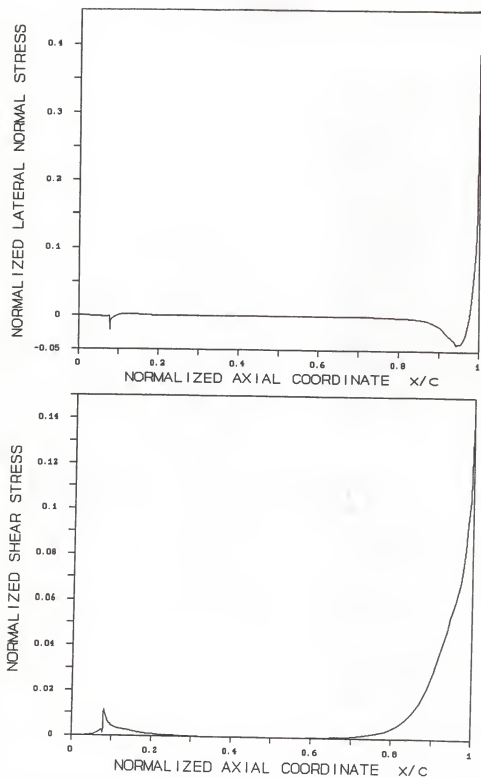
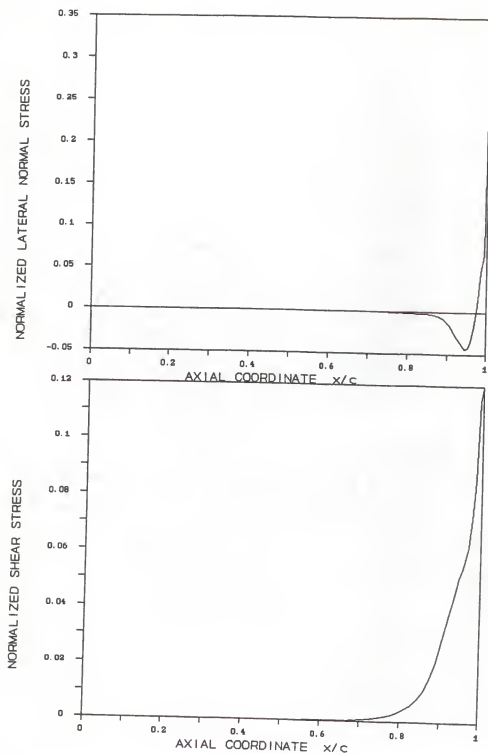Figure 3.31 Case 4. The stress distributions of a double-
doubler joint along the boundary between
the central adherend and lower adhesive
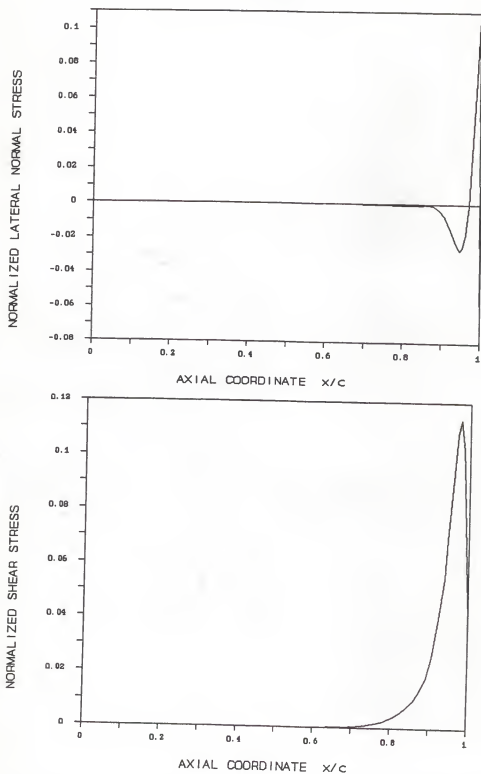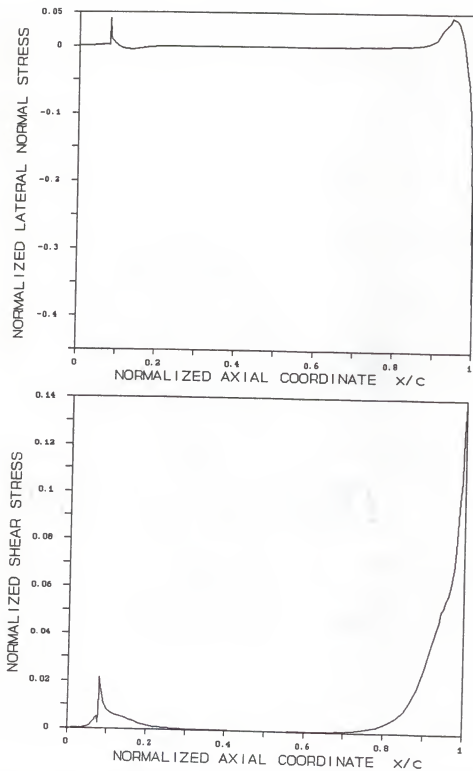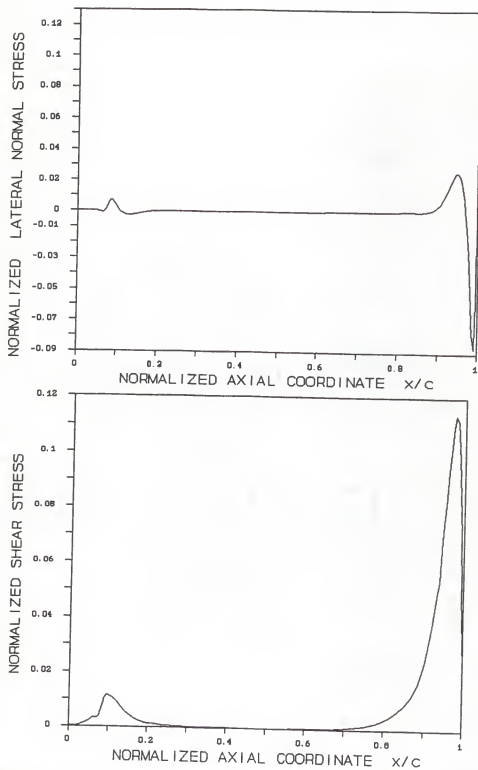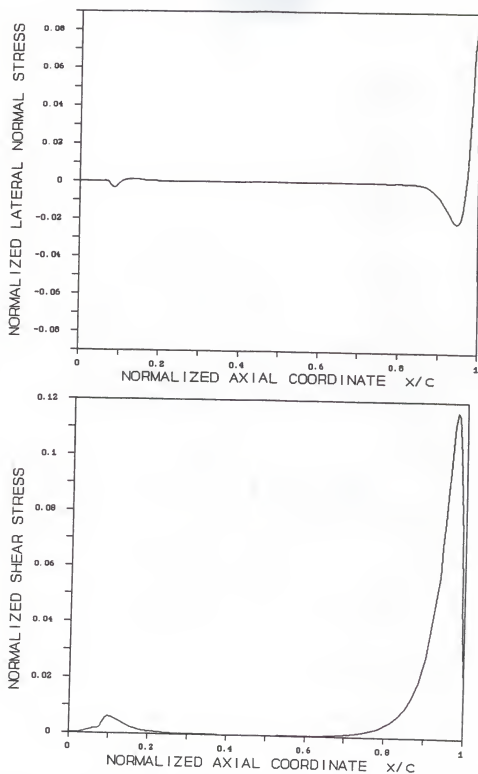
Figure 3.32 Case 4. The stress distributions of a double-doubler joint along the boundary between the lower outer adherend and adhesive

CHAPTER 4
PARAMETRIC STUDY OF THE DOUBLE-DOUBLER JOINT

4.1 Introduction

The objective of this chapter is to study the parameters which influence the stress distributions, so that designers can design the adhesive bonded joints more efficiently. The ANSYS finite element program is used as the computational tool to determine the influence of various joint parameters on stress distributions in the double-doubler joint under tesile loading.

The stress distributions presented in this parametric study are normalized with respect to the applied average stress p_{av} acting on the central adherend. The influence of the parameters is studied by varying one parameter at a time from a double-doubler joint which is described in Figure 3.1.

The geometric and material parameters which are examined are

    a) bonding half length c
    b) the ratio of the adherend modulus to the
       modulus of the adhesive E/E_a

For the material parameter study, the central and outer adherends are made of the same isotropic material.

The thickness of the central adherend, $2t_c$, is constant through the study. All geometric parameters are nondimensionalized by dividing by t_c. Note that $x/c = (x/t_c)/(c/t_c)$. Material parameters are nondimensionalized by dividing the adherend modulus E by the modulus of the adhesive E_a.

The influence of E/E_a on the stresses for simple tension is dicussed in Section 4.2. The influence of the length of overlap on the stresses for simple tension is examined in Section 4.3.

4.2 The Material Parameter

The material parameters consist of the mechanical properties of the adherend and adhesive. The mechanical properties of the any isotropic elastic material are the elastic modulus and the Poisson's ratio. Stresses are affected by variation in Poisson's ratio if the changes in Poission's ratio are very large. Since the range of the variation of Poisson's ratio for common adhesive systems is very limited, only a single material parameter is considered in this analysis. This single material parameter is the ratio of the adherend modulus to the adhesive modulus. To study the influence of the material parameters four joints are analyzed. The adherends in the four joints have four different moduli of elasticity but the same adhesive. The modulus of elasticity is the same for central adherend and outer

adherend. The Poisson ratio of the adherend is constant at 0.33.

The variation in the shear and lateral normal stress distributions in the adhesive are examined for $E/E_a = 1$, $E/E_a = 30$, $E/E_a = 100$, and $E/E_a = 200$. In this study the modulus of the adhesive E_a is 0.356×10^6 psi and the constant Poisson's ratio of the adhesive is 0.39. The stress distribution and singularity parameters in this double-doubler joint are studied for four ratios of E/E_a.

4.2.1 Influence of E/E_a

The influence of the ratio of the modulus of adherends, E, to the modulus of the adhesive, E_a, on the stresses in a double-doubler joint is examined here. The influence of E/E_a on the axial distributions of shear stress at the interface with the center and outer adherend is shown in Figure 4.2 and 4.4, respectively. Each figure consists of two parts. One frame is the neighborhood of the free end surface of the adhesive; the other frame is the neighborhood of the butted adhesive corner. The magnitude of the shear stress decreases rapidly from the neighborhood of the end of adhesive corner and is almost uniform, and equal to the nominal shear stress, over the middle three-fifths of the overlap ($0.2 < x/c < 0.8$ and $-0.2 < x/c < -0.8$). The shear stress then drops to zero at the free end surface of adhesive and outer adherend. As E/E_a increases, the shear stress concentration factor (τ_{max}/τ_{av})

decreases and the order of stress singularity $,\lambda,$ decreases. (See chapter 5.3 for singularity order λ) The magnitude of the highest shear stress is greatest when $E = E_a$.

The location of maximum shear stress is not affected when E/E_a is varied. The variation of stress concentration factor and singularity order λ with respect to E/E_a is given in Table 4.1. The ideal double-doubler joint would have a uniform shear stress distribution and would also have no lateral normal stress. The distributions of lateral normal stress on the boundary between the central adherend and adhesive and between the adhesive and outer adherend are shown in Figure 4.1 and Figure 4.3, respectively. Each figure consists of two parts. One frame is the neighborhood of the free end surface of the adhesive; the other frame is the neighborhood of the butted adhesive corner. The lateral normal stress is tensile on the end of boundary between central adherend and adhesive and is compressive on the end of boundary between adhesive and outer adherend. The lateral normal stresses are almost uniform and almost zero in magnitude over the middle three-fifths of the overlap ($-0.2 < x/c <-0.9$ and $0.2 < x/c < 0.9$) but rise rapidly to tension and compression peaks at the respective ends of the overlap. The axial distribution of lateral normal stress near the free end of the adhesive layer also have tension and compression peaks depending upon the level of y. It is quite obvious that compression and tension lateral normal stress must simultaneously exist in order to

satisfy the vertical equilibrium condition of the adhesive layer. If we assume that the stresses through the adhesive thickness are uniform, we can not predict any compressive lateral normal stress in the adhesive layer. The tensile lateral normal stress concentration factor at the interface between central adherend and adhesive is always greater than that at the interface between adhesive and outer adherend. This concentration factor decreases as E/E_a increases. The greatest concentration factor is obtained at both interfaces for $E = E_a$. It is seen from Figures 4.1 to 4.4 that the magnitude of the maximum lateral normal stress is always greater than the magnitude of the maximum shear stress in a given joint. Therefore the magnitude of the lateral normal stress will be the governing criterion for joint failure in this double-doubler joint.

Table 4.1 Shear stress concentration factor and the order of stress singularity λ for case 1 in Chapter 5.3

	shear stress concentration factor	order of stress singularity λ
$E/Ea = 1$	23.2	0.465
$E/Ea = 30$	3.71	0.355
$E/Ea = 100$	1.95	0.348
$E/Ea = 200$	1.45	0.346

The shear stress concentration factor is calculated with respect to average shear stress
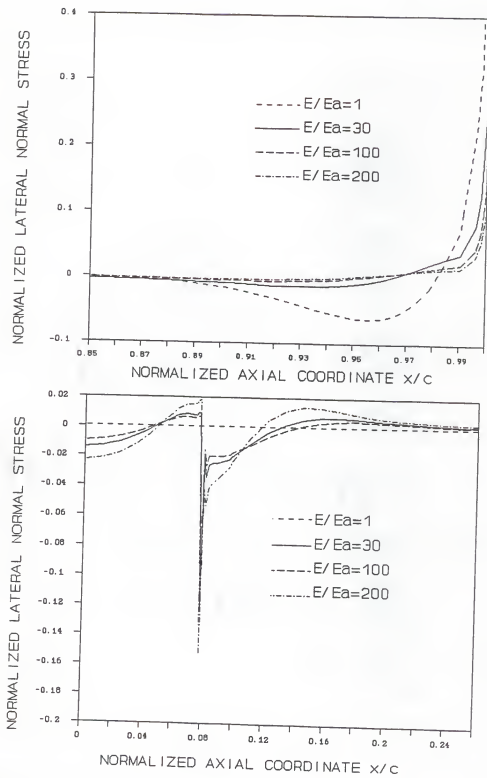
Figure 4.1 Axial lateral normal stress distribution on the boundary between the central adherend and adhesive for four values of E/E_a
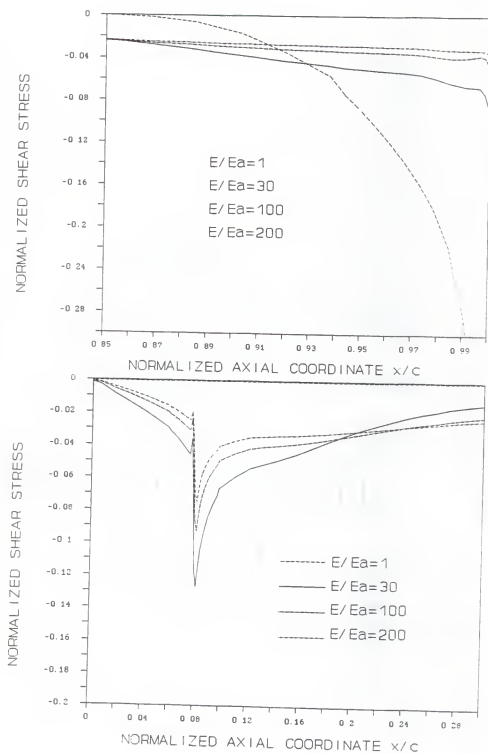
Figure 4.2 Axial shear stress distribution on the boundary between the central adherend and adhesive for four values of E/E_a
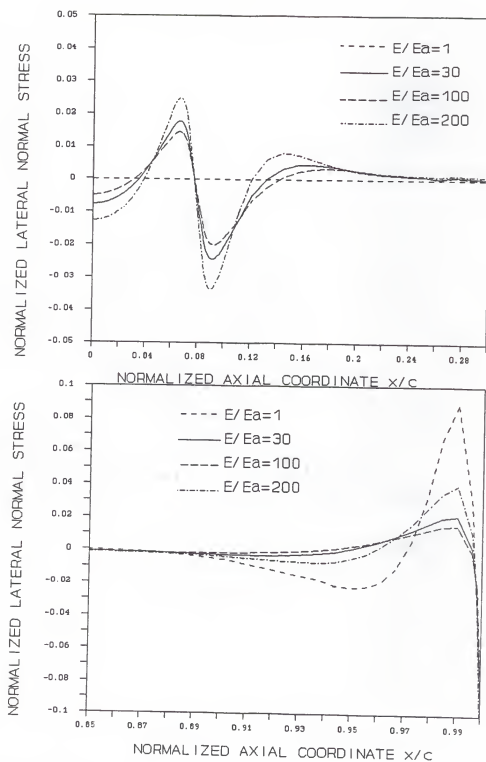
Figure 4.3 Axial lateral normal stress distribution on the
boundary between the outer adherend and adhesive
four values of E/E_a
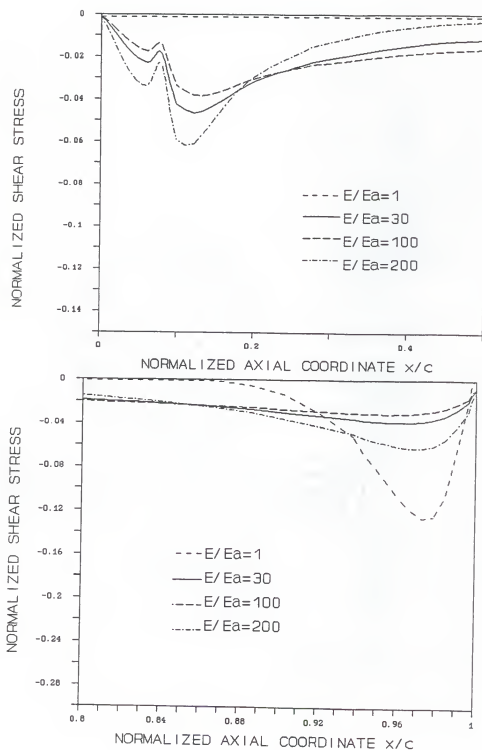
Figure 4.4 Axial shear stress distribution on the boundary between the outer adherend and adhesive for four different values of E/E_a

4.3 The Geometric Parameters

The influence of the geometric parameters is investigated by varying one dimension while all others are held the same as that of original joint. The dimensions of the joint are given in the notation shown in Figure 3.2.

- half length of overlap: $c = 2.56$
- thickness of central adherend: $2t_c = 0.12''$
- thickness of outer adherend: $t_o = 0.04''$
- thickness of adhesive: $t_a = 0.04''$

The thickness of the central adherend is held constant throughout the analysis. The material parameters of the adherends and adhesive are the same for all the joints analyzed for the study of the influence of the geometric parameters:

- adherend modulus: $E = 10.6E6$ psi
- adherend Poisson's ratio: $\nu = 0.33$
- adhesive modulus: $E = 3.6E6$ psi
- adhesive Poisson's ratio $\nu = 0.39$

4.3.1 Influence of Overlap Length

The length of overlap is usually considered to be the most important parameter to the designer. As the applied load is increased, the overlap length must be increased in order to reduce the magnitudes of the average stresses. The stress distributions in three double-doubler joints are analyzed here. All geometries of the three joints are the same as in

original joint (c/t_c = 43) except the overlap lengths which range between c/t_c = 30 and c/t_c = 50.

The shear stress distributions on the boundary between the central adherend and adhesive and between the outer adherend and adhesive for the three double-doubler joints (c/t_c = 30, c/t_c = 43, c/t_c = 50) show that the shear stress concentration factors for the three cases are almost the same. There is no significant difference in stress distribution shape and normalized by p_{av} peak stress values on the range between c/t_c=30 and c/t_c=50. Although the concentration factors are about the same, the actual peak stresses are significantly higher for the shorter overlap, because the average stresses are higher. The lateral normal stress distribution on the boundary between the central adherend and adhesive, and between the outer adherend and adhesive also shows that there is no significant change on the range between c/t_c = 30 and c/t_c = 50. For overlap length c/t_c = 1 (not shown) the highest shear stress occurs at the butt corner of the overlap between two central adherends. As the length of overlap increases significantly, the position of the highest shear stress approaches the ends of the overlap. The maximum lateral normal stress occurs at the ends of the overlap for all three joints.

CHAPTER 5
TREATMENT OF STRESS SINGULARITY
AT BONDING CORNERS IN THE DOUBLE-DOUBLER JOINT

5.1 Introduction

In the linear elastic analysis, stress fields near the two bonding edges between the adherend and the adhesive layer show singular behavior. However, the finite element method solutions provide finite valued stresses at the bonding corners and in these regions the maximum stresses, calculated by the finite element stress analysis, depend on the size of element meshes and are therefore not quite reliable. In order to describe the stress fields around these corners, singular stress parameters are used to evaluate the magnitude of the stress fields near the singularity point of the double-doubler adhesive joint. The assumption is that at some small but finite distance from the singular point where the material is actually elastic, the singularity solution gives a closer approximimation to the stress variation with distance from the corner than the finite element solution does.

This singularity solution method uses two parameters, C_{ij} and $\lambda = 1-p_1$. These parameters express the stress distribution near a bonding edge along the interface, as follows.

$$\sigma_{ij} = C_{ij}/r^{\lambda} \qquad 5.1$$

where

σ_{ij} is stress,

r is distance from singularity point,

C_{ij} is intensity of stress singularity,

λ is order of stress singualrity.

In this chapter the ways to find the C_{ij} and λ for double-doubler joints are presented. For most practical purposes the width of an adhesive joint is large compared to the thickness of the adherend and the adhesive. Therefore plane strain analysis is used throughout.

5.2 Stress Singularities at Interface Corners in Bonded Dissimilar Materials

The typical study of the stress singularity at the interface corner in bonded dissimilar elastic wedges has been done extensively by Bogy [13, 14, 15].

Let D2, D1 denote the open two-dimensional regions occupied by the cross section of the two wedges of angles, a, b, respectively (a+b ≤ 2π), and suppose that they have one straight segment B of their boundaries in common (Figure 5.1). Denote their remaining straight boundary segments by B1, B2. Let (r,θ) be plane polar coordinates of a point with rectangular cartesian coordinates (x,y). The material properties are represented by their respective shear moduli
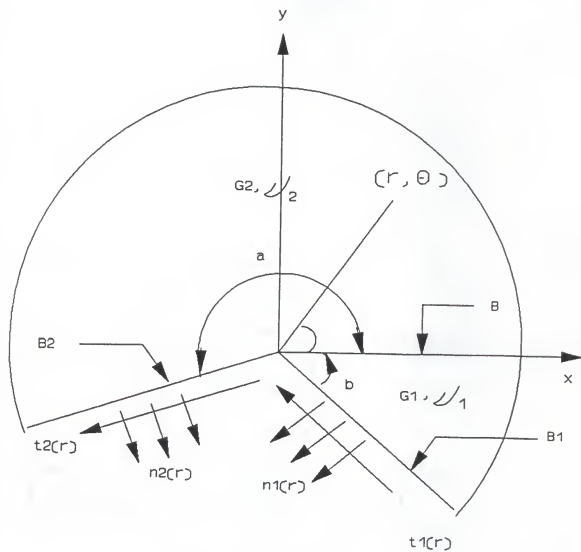
Figure 5.1 Two edge-bonded elastic wedges
of different materials under
normal and shear loading

and Poission's ratios (G_1, ν_1) and (G_2, ν_2). Shear and normal tractions are applied to their free boundaries: $t_1(r)$ and $n_1(r)$ on B1, and $t_2(r)$ and $n_2(r)$ on B2. The traction is independent of the coordinate perpendicular to the cross section. Therefore we consider this boundary value problem in the plane theory of linear elastostatics. The problem now is to find the stress and displacement fields with plane polar components related to the Airy stress function Φ_1, Φ_2, which are suitably defined and satisfy the bi-harmonic equation

$$\nabla^4 \phi = 0 \text{ in D1, D2} \qquad\qquad 5.2$$

The stresses at any point (r, θ) can be derived by

$$\sigma_{rr} = \frac{1}{r} \frac{\partial \phi}{\partial r} + \frac{1}{r^2} \frac{\partial^2 \phi}{\partial \theta^2}$$

$$\sigma_{\theta\theta} = \frac{\partial^2 \phi}{\partial r}$$

$$\sigma_{r\theta} = -\frac{1}{r} \frac{\partial^2 \phi}{\partial r \partial \theta} + \frac{1}{r^2} \frac{\partial \phi}{\partial \theta} \qquad\qquad 5.3$$

$$\frac{\partial u_r}{\partial r} = \frac{1}{2G} \left(\frac{1}{r} \frac{\partial \phi}{\partial r} + \frac{1}{r^2} \frac{\partial^2 \phi}{\partial \theta^2} - (1 - m/4) \nabla^4 \phi \right)$$

where $m = 4(1-\nu)$ for plane strain
$\qquad = 4/(1-\nu)$ for plane stress

$$\frac{\partial u_\theta}{\partial r} - \frac{u_\theta}{r} + \frac{1}{r}\frac{\partial u_r}{\partial \theta} = \frac{1}{G}\left(-\frac{1}{r}\frac{\partial^2 \phi}{\partial r \partial \theta} + \frac{1}{r^2}\frac{\partial \phi}{\partial \theta} \right)$$

which satisfy following boundary conditions on B1, B2

$$(\sigma_1)_{\theta\theta}(r,-b) = n_1(r) \qquad (\sigma_2)_{\theta\theta}(r,a) = n_2(r)$$

$$(\sigma_1)_{r\theta}(r,-b) = t_1(r) \qquad (\sigma_2)_{r\theta}(r,a) = t_2(r)$$

5.4

as well as the conditions of bonding on B (continuity of traction and displacement components)

$$(\sigma_1)_{\theta\theta}(r,0) = (\sigma_2)_{\theta\theta}(r,0) \quad (\sigma_1)_{r\theta}(r,0) = (\sigma_2)_{r\theta}(r,0)$$

$$(u_1)_r(r,0) = (u_2)_r(r,0) \qquad (u_1)_\theta(r,0) = (u_2)_\theta(r,0)$$

5.5

In these equations the subscripts 1 and 2 indicate quantities in wedges I and II, respectively. In addition we shall require the stress components of the two stress fields to specify the regularity conditions

$$\sigma_{rr}, \; \sigma_{\theta\theta}, \; \sigma_{r\theta} = O(r^{-1+\delta}) \text{ as } r \to \infty \text{ for every } \delta > 0 \qquad 5.6$$

The Mellin transform is the most convenient tool for solving the boundary-value problem. We denote the Mellin transform of a function f defined and suitably regular on $(0, \infty)$ by

$$g(f;s) = \int_0^\infty f(r) \; r^{s-1} dr \qquad 5.7$$

where s is the complex transform parameter.

Let $\hat{\phi}(s,\theta)$, $\hat{\sigma}_{rr}(s,\theta)$, $\hat{\sigma}_{\theta\theta}(s,\theta)$, $\hat{\sigma}_{r\theta}(s,\theta)$, $\hat{u}_r(s,\theta)$, $\hat{u}_\theta(s,\theta)$, $\hat{n}(s)$, $\hat{t}(s)$ in this order denote the Mellin transforms with respect to r of $\phi(r,\theta)$, $r^2\sigma_{rr}(r,\theta)$, $r^2\sigma_{\theta\theta}(r,\theta)$, $r^2\sigma_{r\theta}(r,\theta)$, $ru_r(r,\theta)$, $ru_\theta(r,\theta)$, $r^2n(r)$, and $r^2t(r)$.

A formal application of the Mellin transform to Equation 5.2 yields an ordiary differential equation

$$[\frac{d^2}{d\theta^2} + s^2] [\frac{d^2}{d\theta^2} + (s + 2)^2] \; \hat{\phi}(s,\theta) = 0 \qquad 5.8$$

The general solution for this differential equation is given by Bogy [13, 14, 15] by

$$\hat{\phi}(s,\theta) = a(s)\sin(s\theta) + b(s)\cos(s\theta) + c(s)\sin(s + 2\theta)$$
$$+ d(s)\cos(s + 2\theta) \qquad 5.9$$

The functions a(s), b(s), etc., (a1, b1, etc., for $\hat{\phi}_1$ and a2, b2, etc., for $\hat{\phi}_2$) are to be determined through the transforms of Equation 5.3 from the transforms of the boundary condititons Equation 5.4 and Equation 5.5. After use of Equation 5.7 these transformed equations appear as

$$\hat{\sigma}_{rr}(s,\theta) = (\frac{\partial^2}{\partial\theta^2} - s)\,\hat{\phi}(s,\theta)$$

$$\hat{\sigma}_{\theta\theta}(s,\theta) = s(s + 1)\,\hat{\phi}(s,\theta)$$

$$\hat{\sigma}_{r\theta}(s,\theta) = (s+1)\frac{d}{d\theta}\,\hat{\phi}(s,\theta) \qquad\qquad 5.10$$

$$\hat{u}_r(s,\theta) = 1/2G\,[s\,\hat{\phi}(s,\theta) + mc(s)\sin(s\theta+2\theta) + md(s)\cos(s\theta+2\theta)]$$

$$\hat{u}_\theta(s,\theta) = 1/2G\,[-\frac{d}{d\theta}\,\hat{\phi}(s,\theta) + mc(s)\cos(s\theta + 2\theta) - md(s)\sin(s\theta+2\theta)]$$

$$(\hat{\sigma}_1)_{\theta\theta}(s,-b) = \hat{n}_1(s) \qquad (\hat{\sigma}_1)_{r\theta}(s,-b) = \hat{t}_1(s)$$

$$5.11$$

$$(\hat{\sigma}_2)_{\theta\theta}(s,a) = \hat{n}_2(s) \qquad (\hat{\sigma}_2)_{r\theta}(s,a) = \hat{t}_2(s)$$

$$(\hat{\sigma}_1)_{\theta\theta}(s,0) = (\hat{\sigma}_2)_{\theta\theta}(s,0) \qquad (\hat{\sigma}_1)_{r\theta}(s,0) = (\hat{\sigma}_2)_{r\theta}(s,0)$$

$$5.12$$

$$(\hat{u}_1)_r(s,0) = (\hat{u}_2)_r(s,0) \qquad (\hat{u}_2)_\theta(s,0) = (\hat{u}_1)\theta(s,0)$$

By substitution of Equation 5.9 and Equation 5.10 into Equation 5.11 and Equation 5.12, a system of eight equations for the eight unknown functions a1(s), b1(s), c1(s), d1(s), a2(s), b2(s), c2(s), d2(s) is obtained. Then Bogy is concerned with determining the dependence of the order of the singularity in the stress fields as $r \to 0$ on the angle, a, b and the material properties G_1, ν_1, G_2, ν_2. It is shown in reference [13, 14, 15] that the stress fields have a singularity of order r^{-s-2}, log r, or 1 as $r \to 0$ according as the determinant of the coefficient in the system of eight equations has a zero s in $-2 < \text{Re}(s) < -1$, has no zero in this open strip but s = -2 is a zero of order two, has no zero in the strip and s = -2 is only a simple zero. Therefore attention is focused on the determinant of the coefficients in the system of equations with a view toward locating its zeros in $-2 < \text{Re}(s) < -1$. By letting Q denote the value of the determinant of the coefficients of these eight equations the following equation is obtained.

$$Q(a,b,\alpha,\beta;p) = A(a,b;p)\beta^2 + 2B(a,b;p)\alpha\beta + C(a,b;p)\alpha^2$$
$$+2D(a,b;p)\beta + 2E(a,b;p)\alpha + F(a,b;p) \qquad 5.13$$

where

$$A(a,b;p) = 4M(p,a)M(p,b)$$
$$B(a,b;p) = 2p^2\sin^2(a)M(p,b) + 2p^2\sin^2(b)M(p,a)$$
$$C(a,b;p) = 4p^2(p^2-1)\sin^2(a)\sin^2(b) + M[p,(a-b)] \qquad 5.14$$
$$D(a,b;p) = 2p^2[\sin^2(a)\sin^2(pb) - \sin^2(b)\sin^2(pa)]$$

$$E(a,b;p) = -D(a,b;p) + M(p,b) - M(p,a)$$

$$F(a,b;p) = M[p,(a+b)]$$

in which the auxiliary function $M(p,x)$ is defined by

$$M(p,x) = \sin^2(px) - p^2\sin^2(x) \qquad 5.15$$

In Equation 5.13, Equation 5.14 and Equation 5.15 $p = \rho + i\eta$ is a complex varible.

$$\alpha = \frac{G_1m_2 - G_2m_1}{G_1m_2 + G_2m_1} \quad , \quad \beta = \frac{G_1(m_2 - 2) - G_2(m_1 - 2)}{G_1m_2 + G_2m_1} \qquad 5.16$$

where
$$m = 4(1 - \nu) \text{ for plane strain}$$
$$= 4/(1 + \nu) \text{ for generalized plane stress}$$

If we let Q=0 (Equation 5.13) and solve for the smallest value of p, which is called singularity parameter, p_1 , then the orders of singularity in the stress field of wedges I and II are found to be

$$\sigma_1, \ \sigma_2 = \ O(r^{p-1}) \text{ if } p=p_1 \text{ is real}$$
$$O[r^{\xi-1}\cos(\eta_1\log r) \text{ or } r^{\xi-1}\sin(\eta_1\log r)] \qquad 5.17$$
$$\text{if } p_1 = \xi_1 + \eta_1 \text{ is complex}$$

The value of the singularity parameter p_1 in Equation 5.17 is dependent upon the two composite material constants α and β

from Equation 5.16. Stress near the corner point can thus be expressed for real $p_1=p$ as

$$\sigma_{ij} = C''_{ij} f_{ij}(\theta) r^{p-1} \qquad 5.18$$

where C''_{ij} is a constant and $f_{ij}(\theta)$ is a function of θ. Along the interface, $\theta = 0$, stresses do not depend on θ, and we can write

$$\sigma_{ij} = C'_{ij} r^{p-1} \qquad 5.19$$

where $C'_{ij} = C'' f_{ij}(0)$ is a constant. In component form for $\theta = 0$ Equation 5.19 can be written as follows for real $p_1=p$

$$\sigma_x = \sigma_{rr} = C'_x r^{p-1}$$
$$\sigma_y = \sigma_{\theta\theta} = C'_y r^{p-1} \qquad 5.20$$
$$\sigma_{xy} = \sigma_{r\theta} = C'_{xy} r^{p-1}$$

5.3 Calculation of Order and Intensities of Stress Singularities at the Bonding Corners of Double-Doubler Joint

In a double-doubler joint model we can specialize the foregoing discussions for the two different cases.

5.3.1 Case 1. Half Plane Bonded to a Quarter Plane

We have four different locations for this case (Figure 5.2). However, the singularity parameter p_1 has the same value at each of the four locations for the simple tension case because of the symmetric loading and geometric conditions.

The expressions in Equation 5.14 can be written as follows:
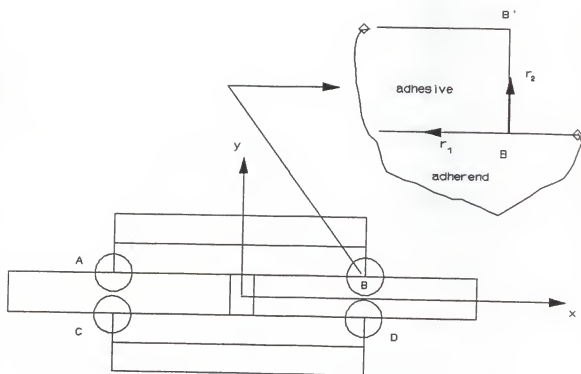
Figure 5.2 Case 1. Half plane bonded to a quarter plane

$$A = 4\sin^2(p\pi)[\sin^2(p\pi/2) - p^2]$$
$$B = 2p^2\sin^2(p\pi)$$
$$C = \sin^2(p\pi/2)$$
$$D = -2p^2\sin^2(p\pi)$$
$$E = (2p^2 - 1)\sin^2(p\pi) + \sin^2(p\pi/2) - p^2$$
$$F = \sin^2(3p\pi/2) - p^2$$

5.21

Substitute this Equation 5.21 into the Equation 5.13. Then Equation 5.13 becomes

$$
\begin{aligned}
Q(\pi,\pi/2,\alpha,\beta;p) = &\; 4\sin^2(p\pi)[\sin^2(p\pi/2 - p^2]\beta^2 \\
&+ 2\times 2p^2\sin^2(p\pi)\alpha\beta + \sin^2(p\pi/2)\alpha^2 \\
&+ 2[-2p^2\sin^2(p\pi)]\beta + 2[(2p^2 - 1)\sin^2(p\pi) \\
&+ \sin^2(p\pi/2) - p^2] + \sin^2(3p\pi/2) - p^2
\end{aligned}
$$

5.22

The solution of $Q=0$ in Equation 5.13 for the smallest p yields the singularity parameter p_1. This parameter p_1 depends on only two factors; the material constants α and β. From the given material properties (Table 5.1), we find the value α and β using the Equation 5.16.

Table.5.1. Selected material properties for singular behavior analysis

material	Young's Modulus	Poission's ratio
Aluminum	10.6E+6 psi	0.33
Epoxy	3.56E+5 psi	0.39

A computer program was written to solve the characteristic equation (Equation 5.22). The Muller method [42] was used for this computer program. This method is used to find any prescribed number of zeros, real or complex, of an arbitrary function.

The values found for α, β are -0.93 and -0.165, respectively. Using these α and β values we find that $p_1 = 0.645$. Then Equation 5.20 can be rewritten in the following form by dividing by the average applied axial normal stress ($p_{av} = p/2t_c$) acting on the central adherend. In the case that r goes in the negative x-direction along the interfacial plane between central adherend and adhesive (r_1 direction in Figure 5.2), the Equation 5.20 can be written in the follwing form. Here the axial normal stress σ_x is not considered since it is not well defined on the interface boundary between central adherend and adhesive.

$$(\frac{\sigma_y}{p_{av}}) = C_y (\frac{r}{c})^{p_1-1} = C_y (\frac{r}{c})^{-0.355}$$

$$5.23$$

$$(\frac{\sigma_{xy}}{p_{av}}) = C_{xy} (\frac{r}{c})^{p_1-1} = C_{xy} (\frac{r}{c})^{-0.355}$$

For the case that r goes in the positive y direction at point B (r_2 direction in Figure 5.2), the Equation 5.20 can be written in the following form. Here we assume that joint boundary BB' is parallel to the y axis at x=2.56. It is found

that σ_x, σ_{xy} are almost zero near the free end of adhesive layer since there is no traction force in the x or y direction on this free end of the adesive layer. Therefore the intensity of stress singularities C_x and C_{xy} are very small. Only the σ_y field is considered.

$$(\frac{\sigma_y}{p_{av}}) \ = \ C_y \ (\frac{r}{t_a})^{p_1-1} = \ C_y \ (\frac{r}{t_a})^{-0.355} \qquad 5.24$$

C_x, C_y, C_{xy} are called the "intensities of stress singularity", which are constant for a specific joint under a specific loading conditions. If we know these factors for a joint, the stresses near the bonding corner along a bond can easily be found by using Equation 5.23 and Equation 5.24. These explicit equations give infinite stress right at the corner. The stress intensity parameters can be used as a means of failure prediction by comparing the calculated parameters with known critical values of these parameters for the material and comparison of stresses very near the bonding corners where stress singularity occur. In order to find the desired intensities of stress singulaity for the double-doubler joint, the following procedure is used.

1) Using the specified boundary displacement (SBD) method described in the following section , calculate stress values for σ_x, σ_{xy}, σ_y from the end of the adhesive interface corner (r/c = 0) to several nodal points in the r_1, r_2 directions,

which are very near the end of the adhesive interface corner. (See Figure 5.2)

2) Substitute these values into equations Equation 5.23 and Equation 5.24, and find several values for C_x, C_y, C_{xy}, respectively.

3) Choose the maximum values from the computed values for C_x, C_y, C_{xy}.

The maximum values are taken as the desired intensities of the stress singularity. Substitution of these values into Equation 5.23 and Equation 5.24 gives a set of stress distributions near the singular point.

5.3.2 Case 2. Three Quarter Plane Bonded to a Quarter Plane
(composite full plane a=3π/2, b=π/2)

In order to apply the same general solution, Equation 5.13, to the neighbourhood of the butted end, it is assumed that the end of the central adherend is de-bonded from the adhesive between the two central adherends. This is equivalent to assuming a straight crack that meets the plane of bond at a=3π/2 and b=π/2. We then have four different singularity locations as with Case 1. (See Figure 5.3)

The singularity parameter p_1 has the same value at each of the four locations for the simple tension case because of the symmetric loading and geometric conditions as Case 1. The expressions in Equation 5.14 can be written as follows.
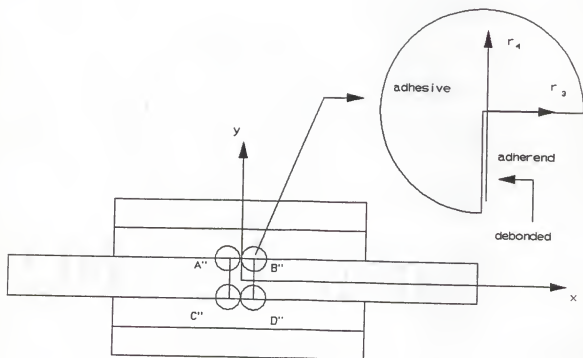
Figure 5.3 Case 2. Three quarter plane bonded to a quarter plane

$$A = 4 \ [\sin^2(3p\pi/2) - p^2][\sin^2(p\pi/2) - p^2]$$

$$B = 2p^2[\sin^2(p\pi/2) + \sin^2(3p\pi/2) - 2p^2]$$

$$C = 4p^2(p^2-1) + [\sin^2(p\pi)]$$

$$D = 2p^2[\sin^2(p\pi/2) - \sin^2(3p\pi/2)] \qquad 5.25$$

$$E = (2p^2-1)[\sin^2(3p\pi/2) - \sin^2(p\pi/2)]$$

$$F = \sin^2(2p\pi)$$

Substitute this Equation 5.24 into the Equation 5.13. Then Equation 5.13 becomes

$$
\begin{aligned}
Q(3\pi/2,\pi/2,\alpha,\beta;p) = & \ 4 \ [\sin^2(3p\pi/2) - p^2][\sin^2(p\pi/2) - p^2]\beta^2 \\
& + 4p^2[\sin^2(p\pi/2) + \sin^2(3p\pi/2) + 2p^2]\alpha\beta \qquad 5.26 \\
& + [4p^2(p^2+1) + \sin^2(p\pi)]\alpha^2 \\
& + 4p^2[\sin^2(p\pi/2) - \sin^2(3p\pi/2)]\beta \\
& + (4p^2+2)[\sin^2(3p\pi/2) - \sin^2(p\pi/2)]\alpha \\
& + \sin^2(2p\pi)
\end{aligned}
$$

The solution of $Q = 0$ for the smallest p yields the singularity parameter p_1. The values found for α, β are $\alpha = -0.93$ $\beta = -0.165$.

Using these α and β values, we find from Equation 5.26 that $p_1 = 0.543$. The same SBD procedure is used to find the desired intensities of stress singularity as was used for Case 1. Then Equation 5.20 can be rewritten in the following form in same way as Case 1. For the case that r goes along the positive x direction of the interface between central adherend

and adhesive from B" (r_3 direction in Figure 5.3), Equation 5.20 can be written in the following form. Here only the axial shear stress σ_{xy} is considered since it is the dominant stress field.

$$(\frac{\sigma_{xy}}{p_{av}}) = C_{xy}(\frac{r}{c})^{p_1-1} = C_{xy} (\frac{r}{c})^{-0.457} \qquad 5.27$$

For the case that r goes along the positive y direction from B" (r_4 direction in Figure 5.3), Equation 5.20 is rewritten in the following form. Axial normal stress (σ_x), shear stress (σ_{xy}) are considered here since these are the major stress fields here.

$$(\frac{\sigma_x}{p_{av}}) = C_x (\frac{r}{t_a})^{p_1-1} = C_x (\frac{r}{t_a})^{-0.457}$$

$$5.28$$

$$(\frac{\sigma_{xy}}{p_{av}}) = C_{xy} (\frac{r}{t_a})^{p_1-1} = C_{xy} (\frac{r}{t_a})^{-0.457}$$

5.4 Specified Boundary Displacement Method (SBD)
5.4.1 Introduction

In many applications of finite element structural analysis, it becomes necessary to determine concentrated stress in a small portion of a structure. The stress field surrounding a sharp fillet is characterized by rapidly

changing stress gradients, which call for a comparatively fine mesh. It can be difficult to include sufficient mesh refinement in an entire model for accurate stress computation at the concentration. One of approaches to this problem is the specified boundary displacement method (SBD).

The specified boundary displacement method is a technique whereby the boundaries of a specialized model of a sub-region within a structure assume the displacement field from a previous solution of the entire structure. The analyses of the subregion and of the entire structure are separate. What is important is that the initial analysis of the entire structure yields an accurate displacement field where the boundaries of the subregion occur and that the analysis of the subregion accurately recovers stress and strain at the points of interest. Analyses of structures containing stress concentration are excellent applications for the specified boundary displacement method. In reality, it can be often observed that the more localized is the effect of a stress concentration, the greater is the need for a specialized model to recover accurate stress and strain. See, for example, [25, 26, 33].

5.4.2 Procedure

Analysis of a stress concentration by the SBD method proceeds as described below and shown in Figure 5.4. This procedure follows that in [33].
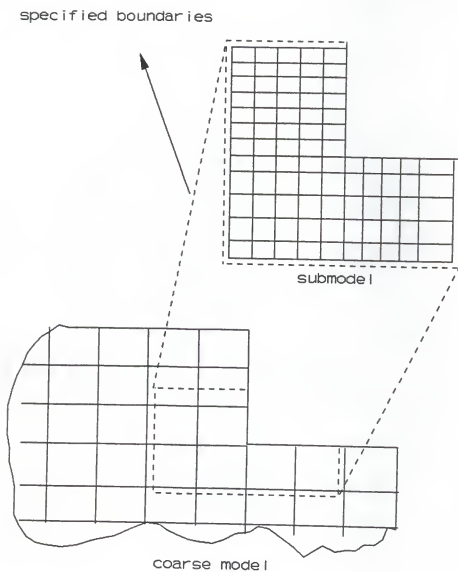
specified boundaries

submodel

coarse model

Figure 5.4 Specified boundary displacement method

1) A finite element model of a large portion of the structure is prepared. This model must have sufficient refinement to obtain the overall displcement field, but need not have sufficient refinement for accurate computation of stress at the concentration. A stress solution is performed for the desired loading with this coarse model.

2) A detailed finite element model of the stress concentration is prepared. This submodel extends some arbitrary distance away from the concentration.

3) Displacements along the specified boundaries of the submodel are obtained from the coarse model solution. For each node along the specified boundary, the appropriate element of the coarse model is determined. The corner displacements of that element are interpolated using its shape function to produce the displacement constraints to be applied to the specified boundary nodes.

4) The submodel stress solution is performed using these interpolated displacements along with any other appropriate boundary conditions.

The SBD method permit independent definition of the coarse and sub models. It allows review of coarse model results before decisions are made about local models.

5.4.3 Benefits of Submodelling

Acoording to [25,26], the benefits of submodelling are that

1) It reduces the need for complicated transition regions in solid finite element models.

2) It enables the analyst to decide which areas of a structure will receive detailed analysis after the initial analysis is complete.

3) It enables the analyst to study the effect of local geometric changes around the stress discontinuity of alternate designs.

4) It enables the analyst to demonstrate the adequacy of mesh refinement.

5) The refined mesh boundary doesn't have to follow coarse mesh element boundaries.

5.4.4 Coarse Model and Submodel

Accurate results can be obtained through the proper selection of coarse model and submodel. Two different coarse models and three different sub-models were prepared for the double-doubler joint. From these models the combination of coarse model and submodel that gave the highest peak stresses was selected. Two cases were considered. The submodel for Case 1 is in the corner at the free end of the adhesive as shown in Figure 5.5. For Case 2 the submodel is in the adhesive near the butted corner of the central adherend, as

shown in Figure 5.6. In both cases the joint is loaded in simple tension. The selected coarse and submodel for Case 1 are shown in Figure 5.5. For Case 2 the same coarse model is used as for Case 1 and another submodel is generated as shown in Figure 5.6. The analysis was carried out using the finite element computer program ANSYS. For the model which is under simple tension loading, only one quarter of the double-doubler joint is selected for this finite element model because of symmetry. For the model which is under pure bending, half of the double-doubler joint will be selected for this finite element model. Both coarse model and sub-model are constructed using ANSYS STIF42, a four-noded isoparametric plane strain element. Using the stress values obtained from the sub-models and substituting these values into Equation 5.23, Equation 5.24, Equation 5.27 and Equation 5.28, we obtain several different values for C_x, C_{xy}, C_y for Case 1 and Case 2 for two different loading cases, respectively. Here only the simple tension loading case is presented to obtain the values for C_x, C_{xy}, C_y because the procedure to obtain these values for pure bending case is exactly the same as for simple tension. The obtained different values are shown in Table 5.2 and Table 5.3 for Case 1, and in Table 5.4, and Table 5.5 for Case 2 for the simple tension loading.
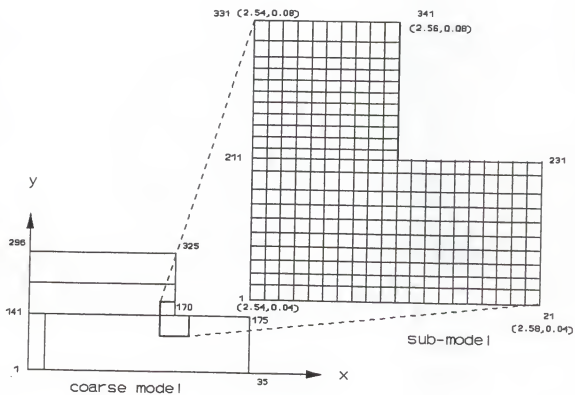
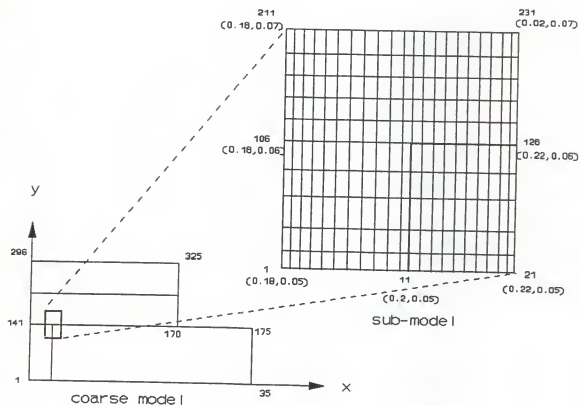Figure 5.5 The Coarse model and sub-model in case 1

Figure 5.6 The coarse model and submodel in case 2

Table 5.2. Different values C_y, C_{xy} for Case 1 in r_1
direction in simple tension loading case

r_1	r_1/c	σ_y/p_{av}	σ_{xy}/p_{av}	C_y	C_{xy}
.002	0.00079	0.2066	0.084	0.014	0.0057
.004	0.00157	0.1434	0.071	0.013	0.0065
.006	0.00236	0.1132	0.068	0.012	0.0072
.008	0.00314	0.09	0.065	0.01	0.0077
.01	0.00394	0.074	0.06	0.0095	0.0077

where r_1 is the distance originating from the end corner of
the adhesive to the negative x direction of interface plane
(See Figure 5.2)

Table 5.3. Different values C_x, C_y, C_{xy} for Case 2 in the
r_2 direction in simple tension loading case

r_2	r_2/t_a	σ_x/p_{av}	σ_y/p_{av}	C_x	C_y
.002	0.033	0.02	0.3312	0.0057	0.094
.004	0.067	0.018	0.1884	0.0066	0.069
.006	0.1	0.002	0.138	0.0008	0.059
.008	0.133	0.002	0.108	0.0009	0.051
.01	0.167	0	0.084	0.0	0.043

where r_2 is the distance originating from the end corner
of the adhesive to positive y direction (See Figure 5.2)

Table 5.4. Different values C_{xy} for Case 1 in the r_3 direction in simple tension loading case

r_3	r_3/c	σ_{xy}/p_{av}	C_{xy}
.004	0.00156	0.273	0.014
.008	0.00312	0.22	0.0157
.012	0.00469	0.178	0.0153
.016	0.00625	0.156	0.0153
.02	0.0078	0.141	0.0153

where r_3 is the distance originating from the
butted corner point to the positive x direction
of interface plane (See Figure 5.3)

Table 5.5. Different values C_x, C_{xy} for Case 2 in the r_4 direction in simple tension loading case

r_4	r_4/t_a	σ_x/p_{av}	σ_{xy}/p_{av}	C_x	C_{xy}
.0025	0.0625	0.3612	0.1512	0.102	0.04
.005	0.125	0.2712	0.07	0.1048	0.027
.01	0.25	0.1888	0.046	0.1	0.024
.015	0.375	0.1332	0.038	0.08	0.024

where r_4 is the distance originating from the butted corner
point to the positive y direction (See Figure 5.3)

From these values, we choose the maximum values in each direction. The maximum values for Case 1 in the r_1 direction are $C_y = 0.014$, $C_{xy} = 0.0077$ and in the r_2 direction $C_y = 0.067$. For Case 2 the maximum values in the r_3 direction are $C_{xy} = 0.016$ and $C_x = 0.105$, and in the r_4 direction $C_{xy} = 0.04$. Substituting these values into Equation 5.23, Equation 5.24, Equation 5.27 and Equation 5.28, we obtain the final equations, which give a set of stress distributions near the singular point as follows.

Case 1 for the simple tension case in the r_1 direction

$$(\sigma_y/p_{av}) = 0.014(r_1/c)^{-0.355}$$

$$5.29$$

$$(\sigma_{xy}/p_{av}) = 0.0077 \ (r_1/c)^{-0.355}$$

Case 1 for the simple tension case in the r_2 direction

$$(\sigma_y/p_{av}) = 0.094 \ (r_2/t_a)^{-0.355} \qquad 5.30$$

Case 2 for the simple tension case in the r_3 direction

$$(\sigma_{xy}/p_{av}) = 0.0157(r_3/c)^{-0.457} \qquad 5.31$$

Case 2 for the simple tension case in the r_4 direction

$$(\sigma_x/p_{av}) = 0.105 \ (r_4/t_a)^{-0.457}$$

$$5.32$$

$$(\sigma_{xy}/p_{av}) = 0.04 \ (r_4/t_a)^{-0.457}$$

CHAPTER 6
RESULTS AND DISCUSSION

6.1 Introduction

The results of finite element stress analysis of a double-doubler adhesive bonded joint are presented in this thesis. Two different loading cases (a simple tension and a pure bending applied at the ends of the adherends) are considered to evaluate the traction distributions on the interfaces and the cohesive stresses in the interior of the adhesive layer. Results of a parametric study of the joint properties is presented to show the influences of the various joint parameters on the stress distributions in the joint. A refined treatment for the stress field near the singular points is presented. A set of "stress singularity parameters" are devised to represent the stresses in the regions close to and including the singular points.

The summary of the results of this analysis is presented in Section 6.2. Suggestions for more efficient joint design are discussed.

Recommendations for future work are in the concluding section, Section 6.3.

117

6.2 Summary and Conclusions

The double-doubler joint with identical adherends and non-identical adherends, shown in Figure 3.1, was analyzed. The computational tool for the analysis is the ANSYS finite element program. All three materials involved are assumed in linear elastic under the applied load. The stress analysis is treated as a plane strain problem. A linear elastic stress analysis of the double-doubler joint is given in Chapter 3. A parametric study of the double-doubler joint is given in Chapter 4, where the influences of two important joint parameters are analyzed. In Chapter 5, "stress singularity parameters" are devised to describe stress fields near the singularity zone.

The important stresses in a double-doubler joint are the shear and lateral normal stresses in the adhesive and axial normal stresses in the adherends. The maximum magnitudes of these stresses and their gradients occur at the end zone of adhesive overlap and at the bonded corner zone at butted region between two central adherends in the simple tension case. In the pure bending case the maximum magnitude of these stresses and their gradients occur at the end zone of adhesive over lap. The critical areas of the adhesive are, therefore, at the ends of the overlap and at the bonded corner of butted region.

These critical areas extend over approximately 10% of the overlap length at the ends of the overlap and 10% of the

overlap length at the bonded corner of the butted region. The axial distributions of stress (σ_x, σ_y, σ_{xy}) in the adhesive are almost uniform at a low level over the middle 75% of overlap. The axial normal stress distribution in the adhesive layer varies linearly through the adhesive layer thickness near the end. Along the boundary between the central adherend or outer adherend and adhesive, axial normal stress (σ_x) is not well defined. Therefore one would not expect the free end condition ($\sigma_x = \sigma_{xy} = 0$) to be satisfied at the very near end zone. However, the end condition ($\sigma_x = \sigma_{xy} = 0$) at the various levels inside the adhesive, which means no external traction force in the x or y direction on the end, is almost satisfied by using the displacement finite element method.

The lateral normal stress has its highest peak value at the edge of the interface between the central adherend and adhesive. The lateral normal stress (σ_y) becomes compressive in part of the upper level of adhesive near the interface between the adhesive and outer adherend, and at that interface it shows an interval of very high compressive stress. If we assume that stresses through the adhesive thickness are uniform, we can not predict the compressive lateral normal stress regions of the adhesive layer.

From the parametric study of the joint with adherends of the same isotropic material, it is concluded that the single most important parameter influencing the stresses is the ratio of the adherend modulus to the modulus of the adhesive, E/E_a.

The stresses in the adherends and adhesive are influenced by change in E/E_a. The stress peaks are greatest when $E/E_a = 1$ and decrease with increase in E/E_a. The stresses in the adhesive and adherends do not change appreciably for values of $E/E_a > 100$.

The influence on the stress peaks due to change in overlap length, 2c, is similar to the influence of E/E_a. As c/t_c increases, the peak stresses and stress gradients decrease in magnitude.

The stress singularity parameters together with the order of singularity fully describe the stress fields near the ends of adhesive overlap and at the bonded corner of the butted region between two central adherends:

$$\sigma_{ij}/P_{av} = C_{ij} \; (r/c)^{p-1}$$

where C_{ij} are the stress singularity parameters and (p-1) is the singularity order (the strength of the singularity). The singularity at the bonding corners of two different materals depends on the materal constants α and β (Equation 5.16), which are functions of Young's moduli and Poisson's ratios of the adhesive and adherends. The strength of the singularity (singularity order) $\lambda = p-1$ decreases as the ratio, E/E_a, increases. The singularity order, λ, increment is very small over the range $E/E_a > 50$ and is noticeable below the range $E/E_a < 30$. Efficient double-doubler joints can be designed based on a study of these influences. The parameters of the joint actually designed will depend on the particular

design requirements and the functions the joint has to accomplish.

In the model of adhesive bonded joints for finite element analysis, it is important that the critical regions of the adhesive be modeled with very small elements. It has been shown that the stress gradients are high over the 10% of the overlap length at each end of the overlap. Additionally, 5% of the overlap length at each end of the overlap and 15% of the adhesive thickness from each interface must be modeled with several elements in order to get more accurate peak stress near the boundaries.

The specified boundary displacement method for analyzing fine-mesh submodels in the critical region is an efficient method for solving such problem.

6.3 Recommendations for Future Work

The double-doubler bonded joint with linear elastic adhesives was analyzed in this study. Future study should be extended to joints with viscoelastic adhesives subjected to constant thermal stresses, transient thermal stresses and to dynamic loads. The stress singularity parameters may be considered as a means of failure prediction of an adhesive joint by comparing the calculated parameters with known critical values of these parameters for the material. It should be pointed out, however, that this kind of comparison can be made only for machined joints where contact angles

between the adherends and the adhesive layer do not vary (e.g., 90° for the model of this study).

In actual manufacturing processes, however, the uniform contact angles do not occur naturally. Further study should be done to evaluate singularity for different shapes of edge corner with identical anisotropic adherends. Some shape optimization technique could be used to reduce the singularity. Furthermore, the stress singularity problem is encountered only in the linear elastic stress analysis. If yielding occurs during the loading process, the maximum stress concentrations will be significantly reduced due to plastic deformation. This should be further studied.

APPENDIX A
CASE 1. THE AXIAL STRESS DISTRIBUTIONS OF DOUBLE-DOUBLER
        REINFORCEMENT OF A CONTINOUS MEMBER AT DIFFERENT
        LEVELS OF Y
        (ALUMINUM ADHERENDS AND EPOXY ADHESIVE
         IN SIMPLE TENSION)
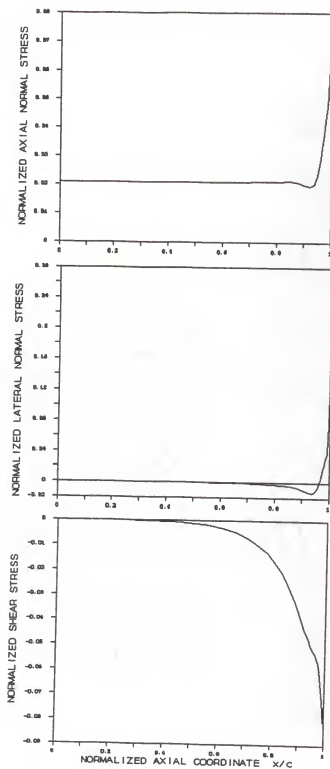
Figure A.1 Case 1. Stress distributions of double-doubler
reinforcement of a continous member at the level
of y=0.06375
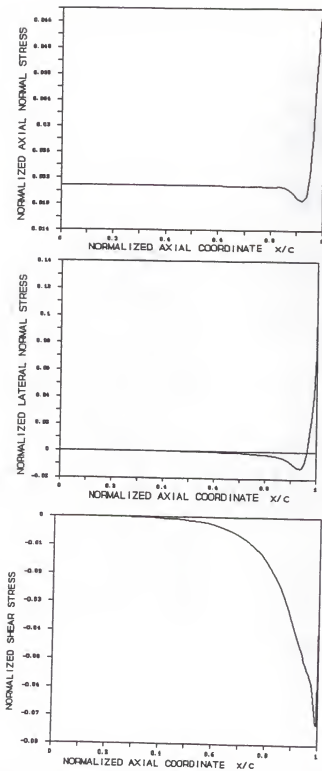
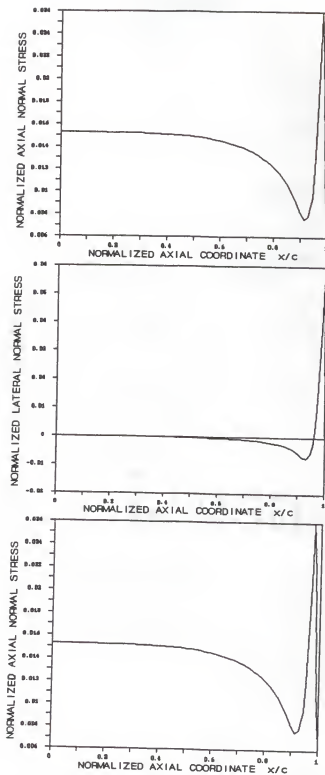Figure A.2 Case 1. Stress distributions of double-doubler of reinforcement of a continous member at the level of y=0.0675
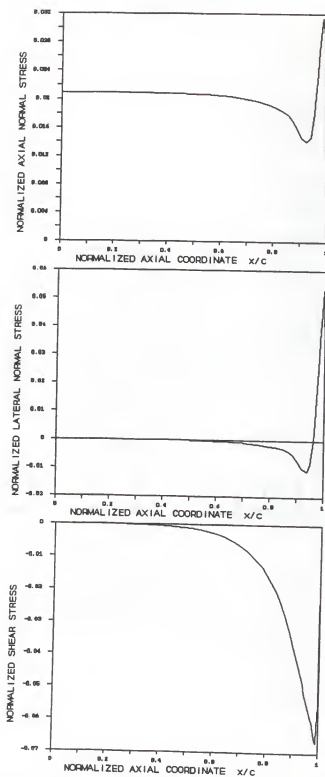
Figure A.3 Case 1. Stress distributions of double-doubler reinforcement of a continous member at the level of y=0.08
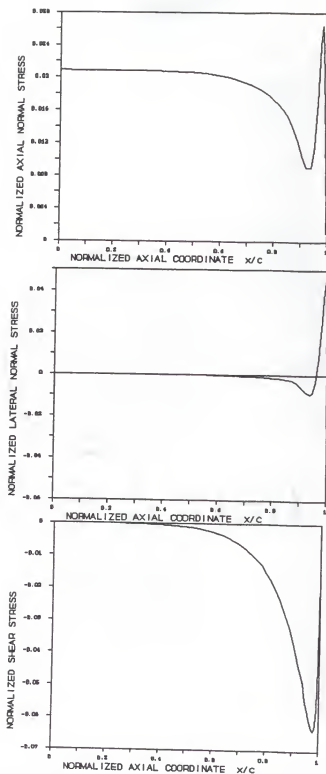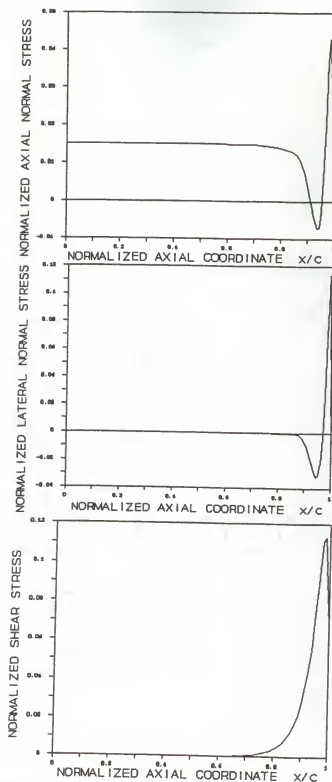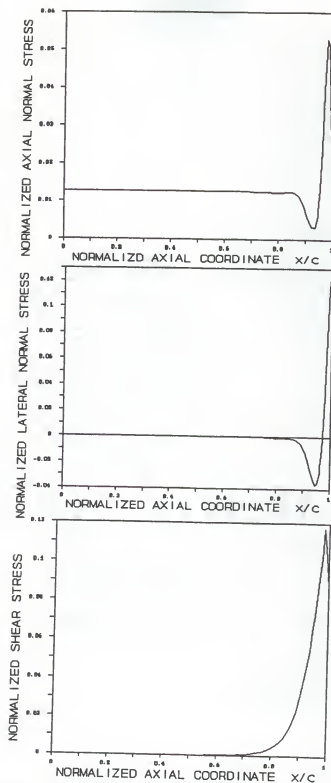
Figure A.4 Case 1. Stress distributions of double-doubler reinforcement of a continous member at the level of y=0.0925

APPENDIX B
CASE 1. THE AXIAL STRESS DISTRIBUTIONS OF A DOUBLE-
DOUBLER JOINT AT DIFFERENT LEVELS OF Y
(ALUMINUM ADHERENDS AND EPOXY ADHESIVE
IN SIMPLE TENSION)
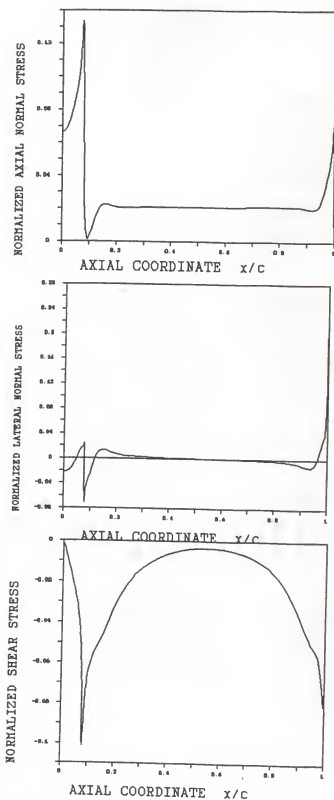
Figure B.1 Case 1. Stress distributions of a double-doubler
joint at the level of y=0.06375
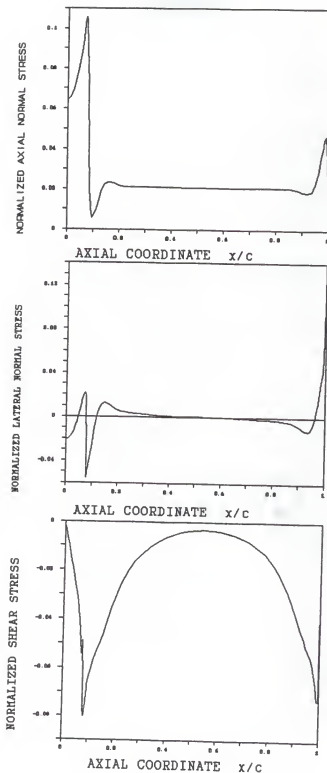
Figure B.2 Case 1; Stress ditributions of a double-doubler
joint at the level of y=0.0675
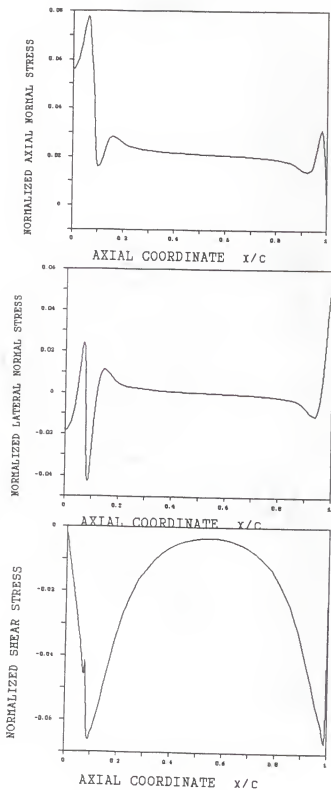
Figure B.3 Case 1; Stress distributions of a double-doubler
joint at the level of y=0.08
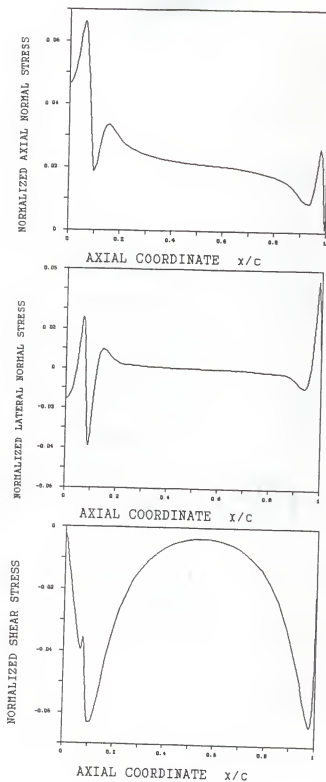
Figure B.4 Case 1. Stress distributions of a double-doubler
joint at the level of y=0.0925

APPENDIX C
CASE 2. THE AXIAL STRESS DISTRIBUTIONS OF DOUBLE-DOUBLER
         REINFORCEMENT OF A CONTINOUS MEMBER AT DIFFERENT
         LEVELS OF Y
         (ALUMINUM CENTRAL ADHEREND, EPOXY ADHESIVE AND
          COMPOSITE OUTER ADHEREND IN SIMPLE TENSION)
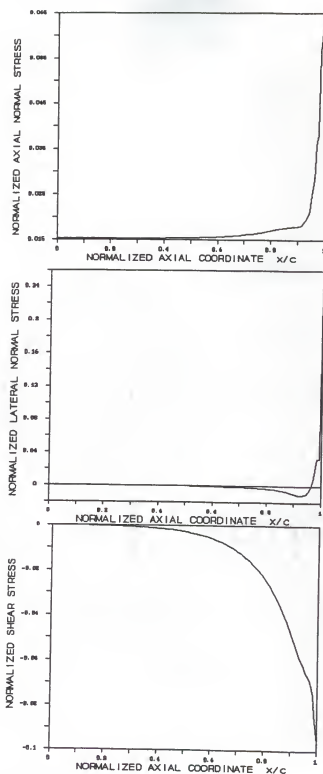
Figure C.1 Case 2. Stress distributions of double-doubler
reinforcement of a continous member at the level
of y=0.06375
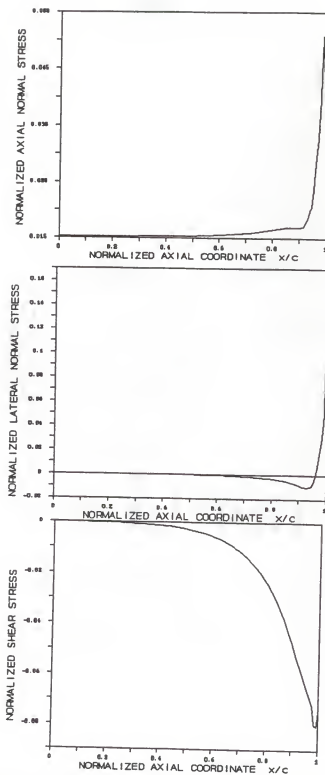
Figure C.2 Case 2. Stress distributions of double-doubler reinforcement of a continous member at the level of y=0.0675
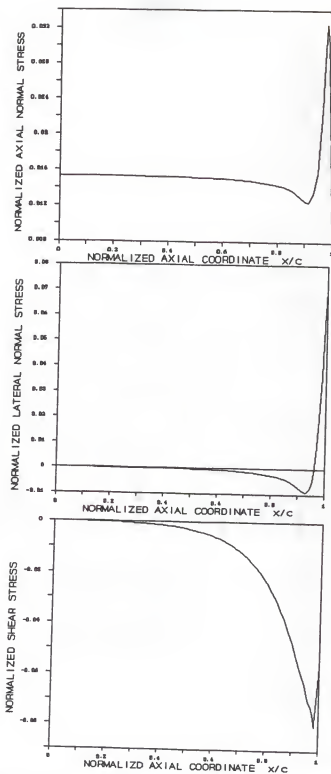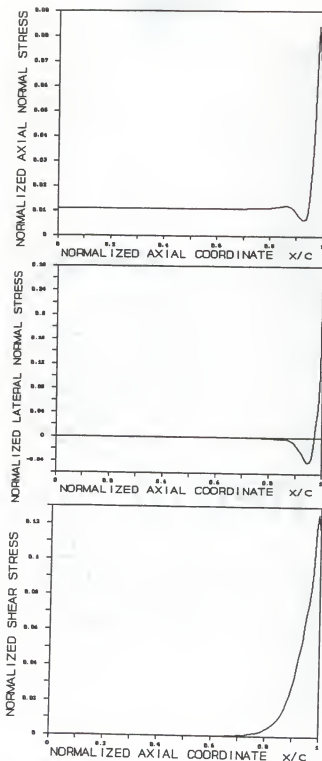
Figure C.3   Case 2. Stress distributions of double-doubler
              reinforcement of a continous member at the level
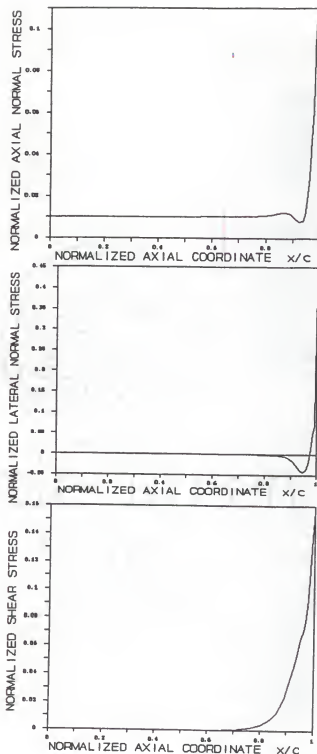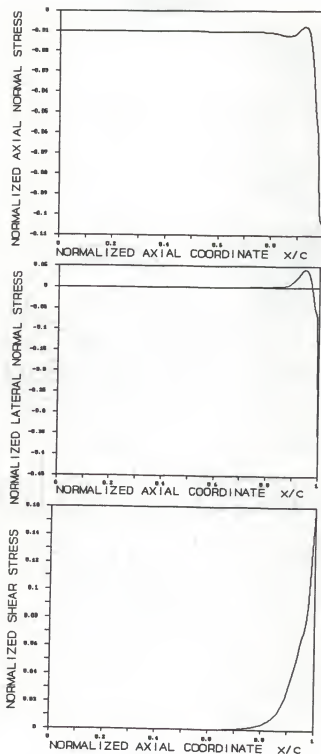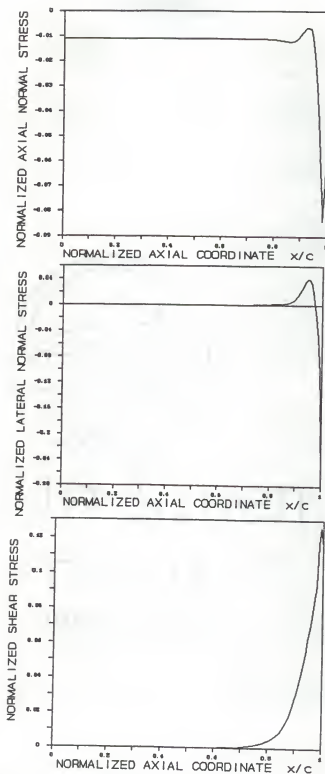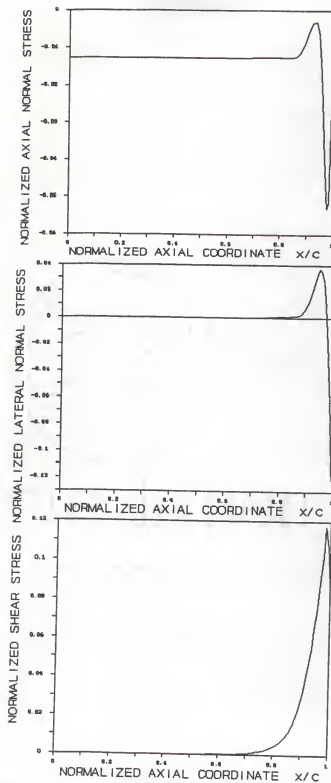   of y=0.08

Figure C.4 Case 2. Stress distributions of double-doubler
reinforcement of a continous member at level of
y=0.0925

APPENDIX D
CASE 2. THE AXIAL STRESS DISTRIBUTIONS OF A DOUBLE-DOUBLER
        JOINT AT DIFFERENT LEVELS OF Y
        (ALUMINUM CENTRAL ADHEREND, EPOXY ADHESIVE, AND
        COMPOSITE OUTER ADHEREND IN SIMPLE TENSION)
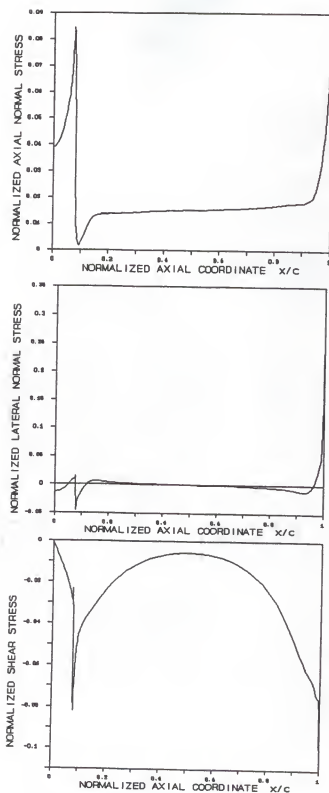
Figure D.1 Case 2. Stress distributions of a double-doubler
joint at the level of y=0.06375
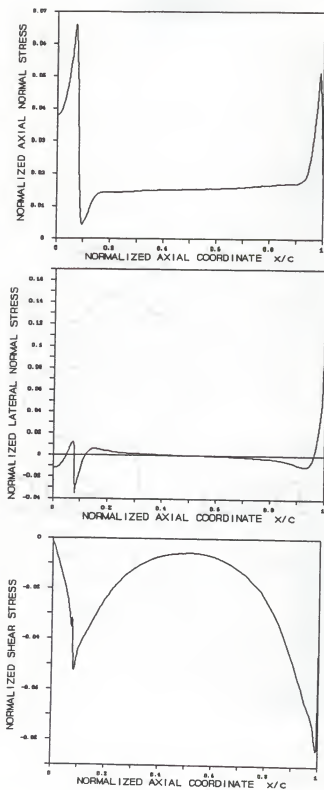
Figure D.2 Case 2. Stress distributions of a double-doubler
joint at the level of y=0.0675
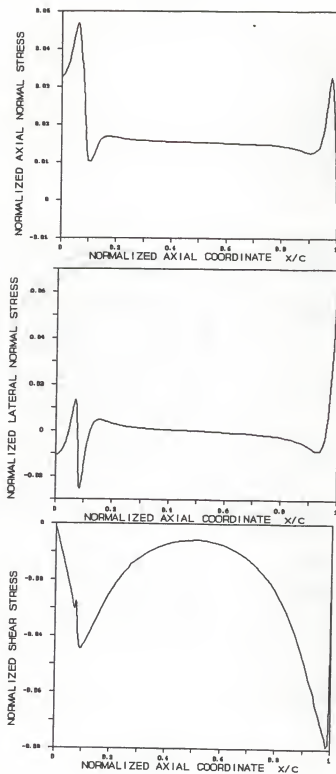
Figure D.3 Case 2. Stress distributions of a double-doubler
joint at the level of y=0.08
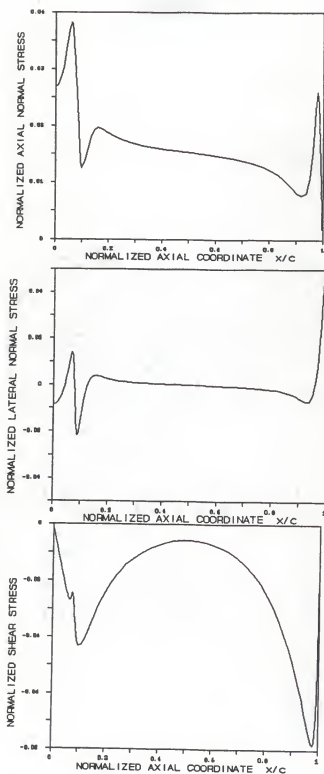
Figure D.4 Case 2. Stress distributions of a double-doubler
joint at the level of y=0.0925

APPENDIX E

CASE 3. THE AXIAL STRESS DISTRIBUTIONS OF DOUBLE-DOUBLER
REINFORCEMENT OF A CONTINOUS MEMBER AT DIFFERENT
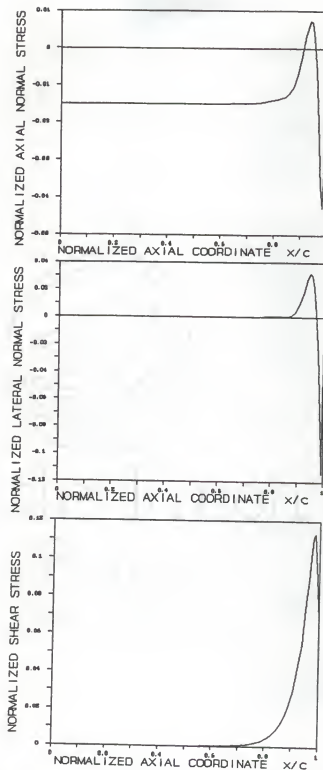LEVELS OF Y
(ALUMINUM ADHERENDS AND EPOXY ADHESIVE
IN PURE BENDING)

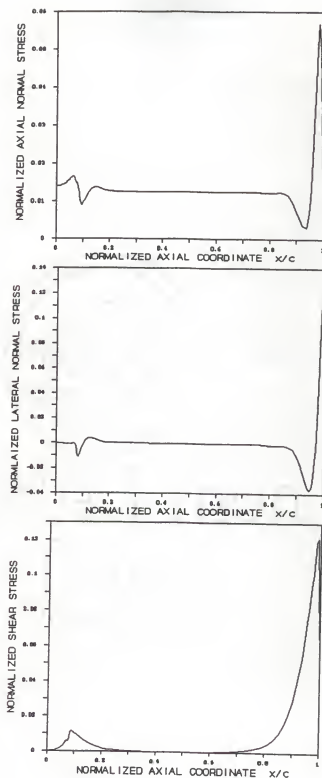Figure E.1 Case 3. Stress distributions of double-doubler
reinforcement of a continous member at the level
of y=-0.095

Figure E.2 Case 3. Stress distributions of double-doubler
reinforcement of a continous member at the level
of y=-0.08

Figure E.3 Case 3. Stress distributions of double-doubler
reinforcement of a continous member at the level
of y=-0.07

Figure E.4 Case 3. Stress distributions of double-doubler
reinforcement of a continous member at the level
of y=-0.065

Figure E.5 Case 3. Stress distributions of double-doubler
reinforcement of a continous member at the level
of y=0.065

Figure E.6 Case 3. Stress distributions of double-doubler reinforcement of a continous member at the level of y=0.07

Figure E.7 Case 3. Stress distributions of double-doubler
reinforcement of a continous member at the level
of y=0.08

Figure E.8 Case 3. Stress distributions of double-doubler
reinforcement of a continous member at the level
of y=0.095

APPENDIX F
CASE 3. THE AXIAL STRESS DISTRIBUTIONS OF A DOUBLE-DOUBLER
JOINT AT DIFFERENT LEVELS OF Y
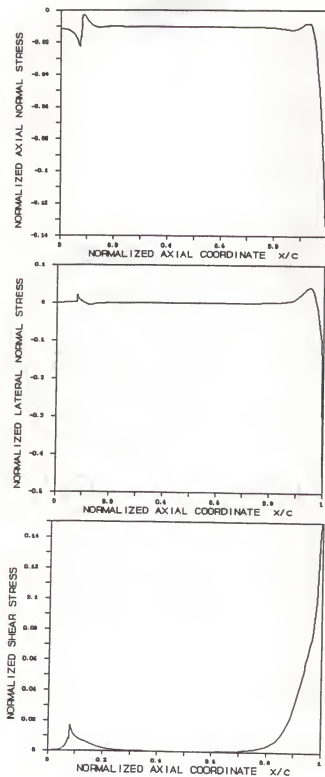(ALUMINUM ADHERENDS AND EPOXY ADHESIVE
IN PURE BENDING)
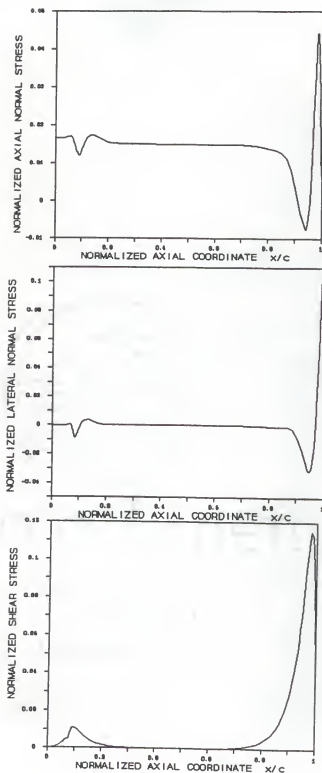
Figure F.1 Case 3; Stress distributions of a double-doubler
joint at the level of y=-0.095

Figure F.2 Case 3. Stress distributions of a double-doubler
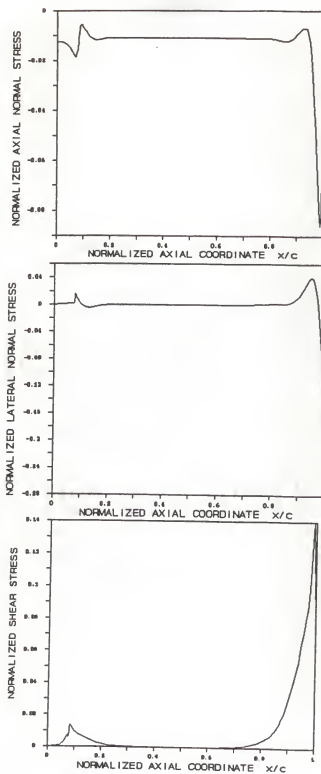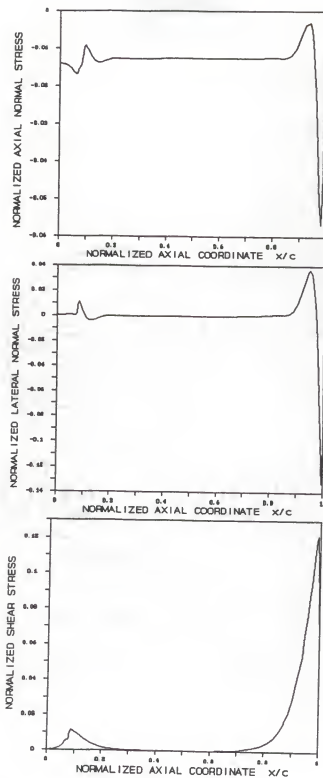joint at the level of y=-0.08
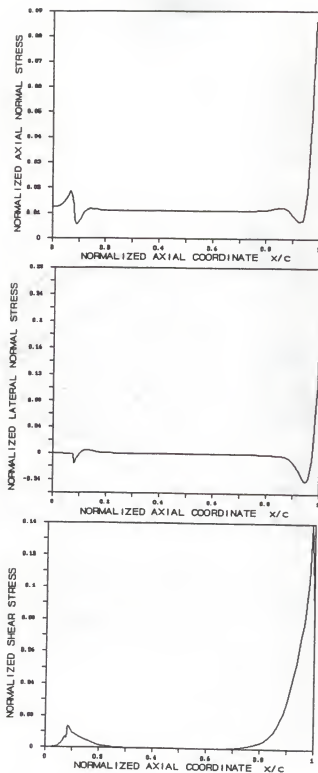
Figure F.3 Case 3. Stress distributins of a double-doubler joint at the level of y=-0.07
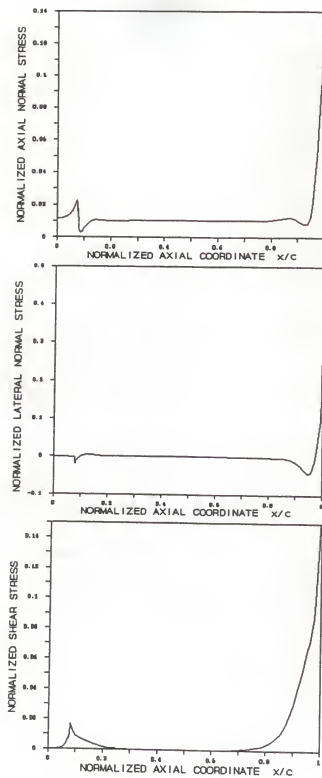
Figure F.4 Case 3. Stress distributions of a double-doubler
joint at the level of y=-0.065

Figure F.5 Case 3. Stress distributions of a double-doubler
joint at the level of y=0.065

Figure F.6 Case 3. Stress distributions of a double-doubler
joint at the level of y=0.07

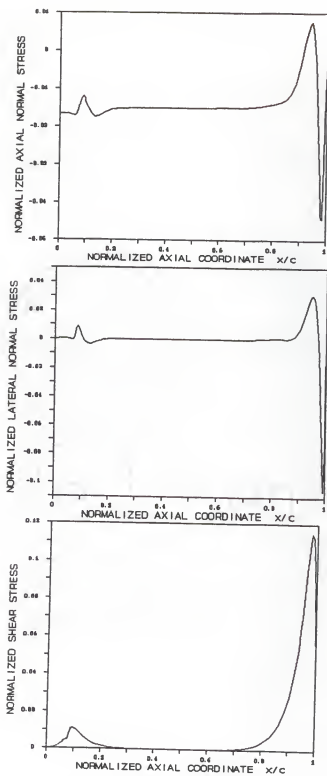Figure F.7 Case 3. Stress distributions of a double-doubler
joint at the level of y=0.08

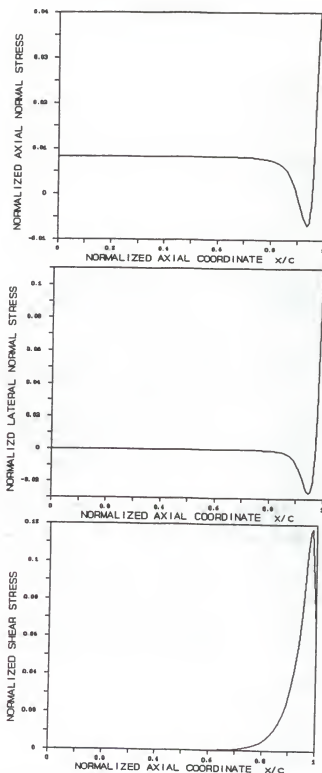Figure F.8 Case 3. Stress distributions of a double-doubler
joint at the level of y=0.0925

Figure G.1 Case 4. Stress distributions of double-doubler
reinforcement of a continous member at the level
of y=-0.095

Figure G.2 Case 4. Stress distributions of double-doubler reinforcement of a continous member at the level of y=-0.08

Figure G.3 Case 4. Stress distributions of double-doubler
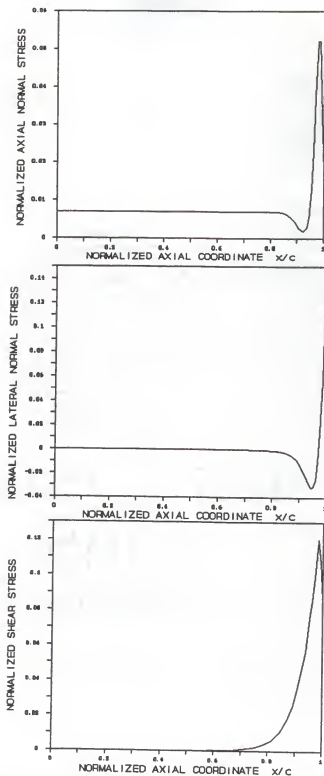reinforcement of a continous member at the level
of y=-0.07

Figure G.4 Case 4. Stress distributions of double-doubler
reinforcement of a continous member at the level
of y=-0.065

Figure G.5 Case 4. Stress distributions of double-doubler
reinforcement of a continous member at the level
of y=0.065

Figure G.6 Case 4. Stress distributions of double-doubler
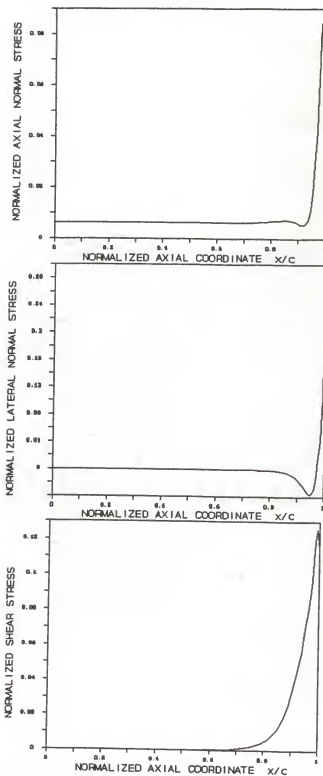reinforcement of a continous member at the level
of y=0.07
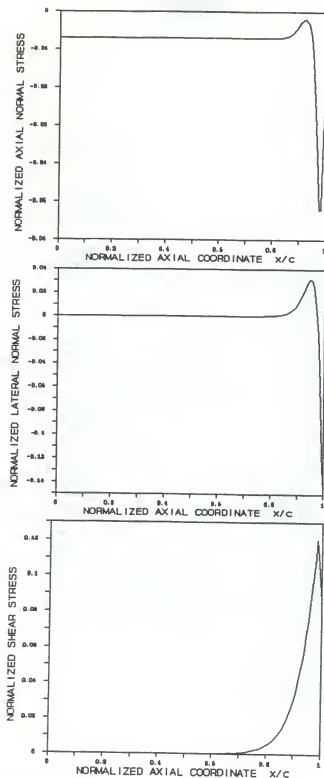
Figure G.7 Case 4. Stress distributions of double-doubler
reinforcement of a continous member at the level
of y=0.08
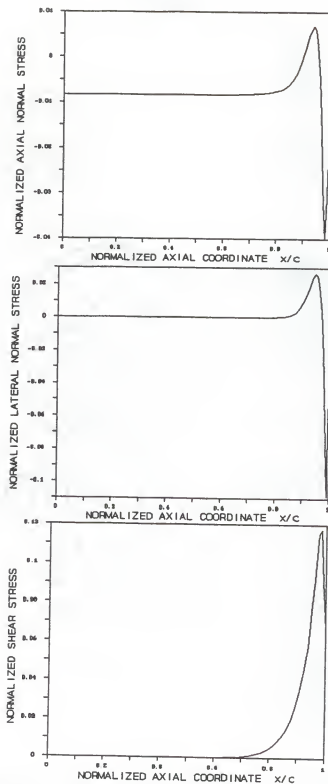
Figure G.8 Case 4. Stress distributions of double-doubler
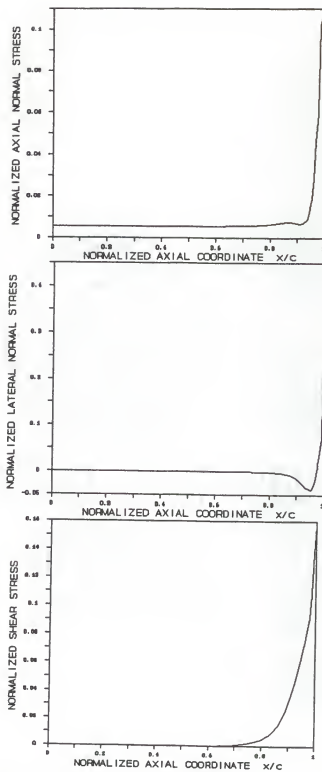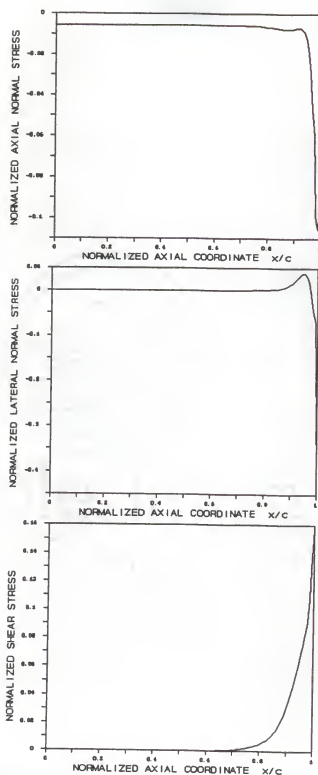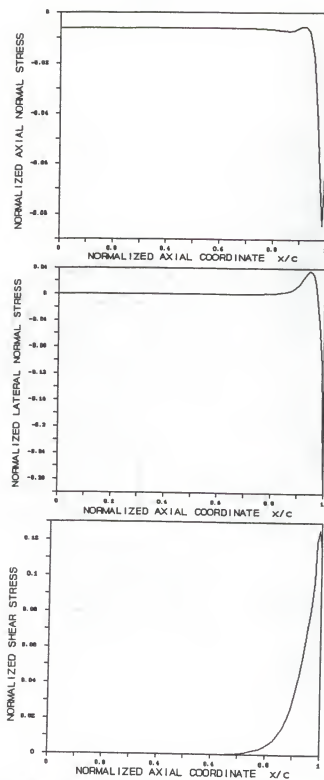reinforcement of a continous member at the level
of y=0.095

CASE 4; THE AXIAL STRESS DISTRIBUTIONS OF A DOUBLE-DOUBLER
JOINT AT DIFFERENT LEVELS OF Y
(ALUMINUM CENTRAL ADHEREND, EPOXY ADHESIVE, AND
COMPOSITE OUTER ADHEREND IN PURE BENDING)

Figure H.1 Case 4. Stress distributions of a double-doubler
joint at the level of y=-0.095

171

Figure H.2 Case 4; Stress distributions of a double-doubler
joint at the level of y=-0.08

Figure H.3 Case 4. Stress distributions of a double-doubler
joint at the level of y=-0.07

Figure H.4 Case 4. Stress distributions of a double-doubler
joint at the level of y=-0.065

Figure H.5 Case 4. Stress distributions of a double-doubler
joint at the level of y=0.065

Figure H.6 Case 4. Stress distributions of a double-doubler
joint at the level of y=0.07

Figure H.7 Case 4. Stress distributions of a double-doubler joint at the level of y=0.08

Figure H.8 Case 4. Stress distributions of a double-doubler
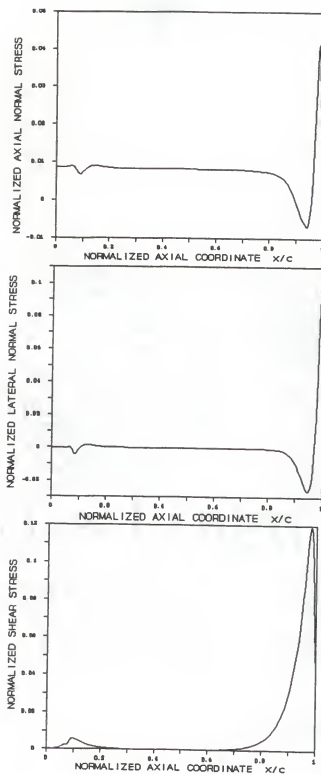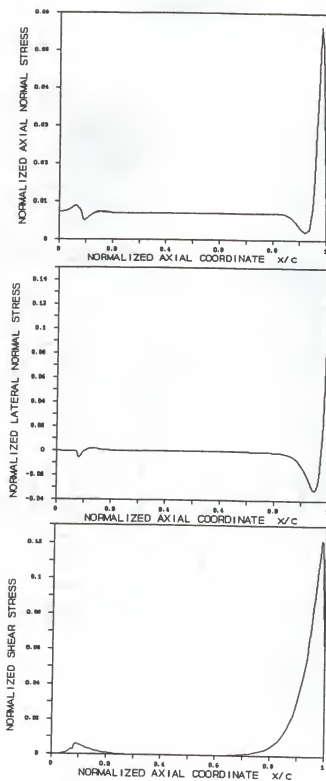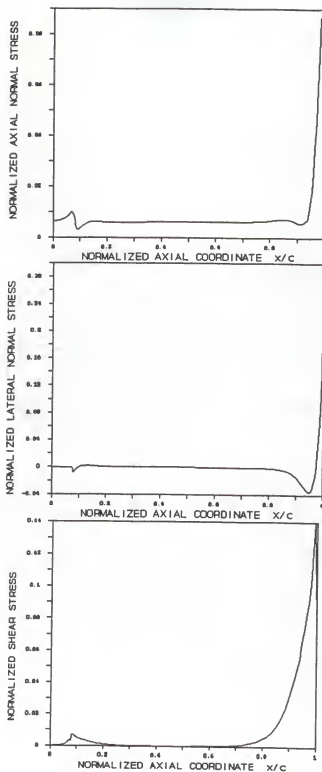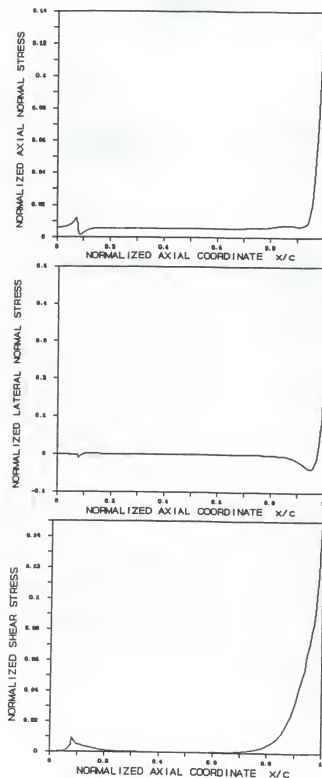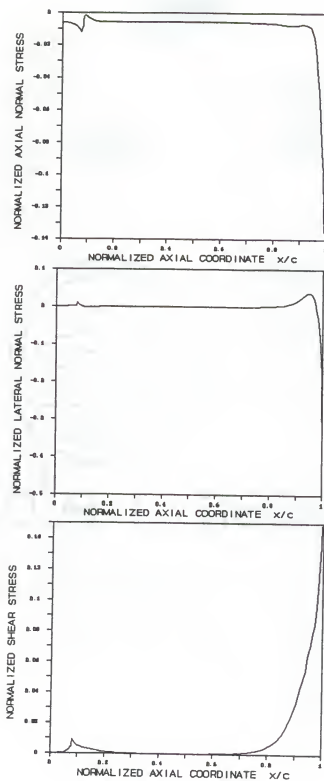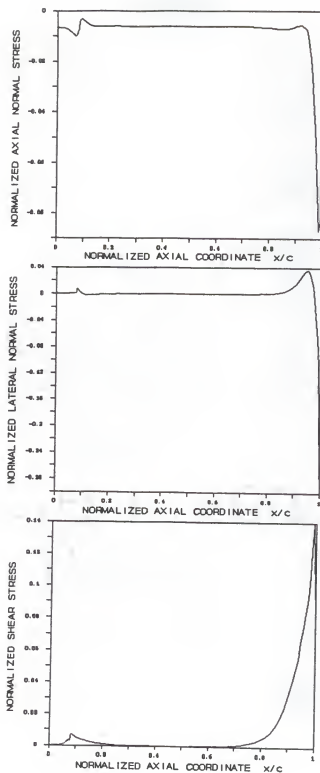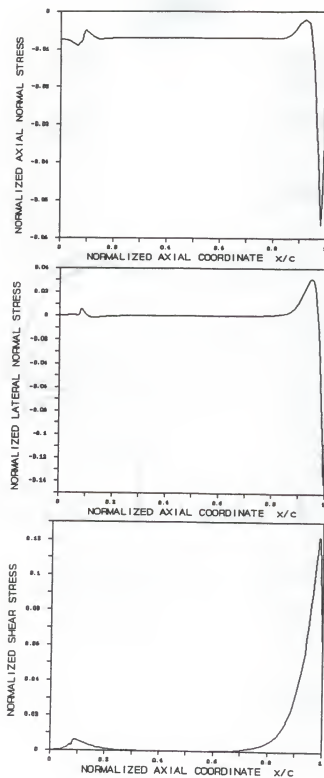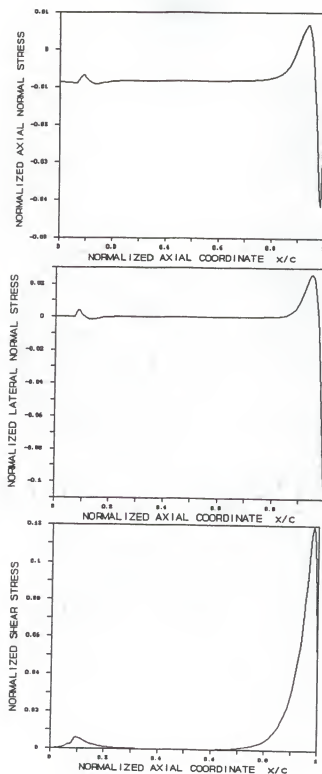joint at the level of y=0.095

LIST OF REFERENCES

[1] O. Volkersen, "Die Nietkraftverteilung in Zugbeanpruchten Nietverbindungen mit Konstanten Laschenquerschnitten," _Luftfahrtforschung_, 1938, pp. 41-47.

[2] M. Goland and E. Reissner, "The Stresses in Cemented Joints," _Journal of Applied Mechanics,_ 1944, pp. A17-A27

[3] F. J. Plantema, _De Schuifspanning in een Lijmnaad_, National Luchtvaartlaboratorium, Amsterdam, Report M1181, 1949.

[4] S. Kelsey, and N. K. Benson, Institut fur Statik und Dynamik, Technische Hochschule, Stuttgart, ISD Report No. 10, 1966.

[5] M. K. Pahoja, _Stress Analysis of as Adhesive Lap Joint Subjected to Tension, Shear Force and Bending Moments_, Ph.D. Thesis and T.& A.M. Report No.361, Department of Theoretical and Applied Mechanics, University of Illinois at Urbana-Champaign, 1972.

[6] W. J. Renton and J. R. Vinson, _The Analysis and Design of Anisotropic Bonded Joints_, Report No. 2, University of Delaware, Newark, Delaware; Air Force Office of Scientific Research, Scientific Report AFOSR TR 75-0125, August 1974.

[7] W. J. Renton and J. R. Vinson, "The Efficient Design of Adhesive Bonded Joints," _Journal of Adhesion_, March 1975, pp. 175-193.

[8] L. J. Hart-Smith, _Adhesive-Bonded Double-Lap Joints_, McDonnell Douglas Corporation, Long Beach, California, NASA CR-112235, January 1973.

[9] K. S. Ahluwalia, _Stress Analysis of Double Shear Bonded Joints by the Finite Element Method_, Master's Thesis, Engineering Science Department, Louisiana State University, Baton Rouge, Louisiana, January, 1969.

[10] G. R. Wooley and D. R. Carver, "Stress Concentration Factors for Bonded Lap Joints," _Journal of Aircraft_, October 1971, pp. 817-820.

[11] A. S. McLaren and I. MacInnes, "The Influence on the Stress Distribution in an Adhesive Lap Joint of Bending of the Adherend Sheets," British Journal of Applied Mechanics, Vol. 9, February 1958, pp. 72-77.

[12] I. Tuzi and H. Shimada, "Photoelastic Investigation of the Stress Distribution in Cemented Joints," Bulletin of Japanese Society of Mechanical Engineers, Vol.7, No.26, 1964, pp. 263-267.

[13] D. B. Bogy, "Edge-Bonded Dissimilar Orthogonal Elastic Wedges Under Normal and Shear Loading," Journal of Applied Mechanics, September 1968, pp. 460-466.

[14] D. B. Bogy and K. C. Wang, "Stress Singularities at Interface Corners in Bonded Dissimilar Isotropic Elasic Materials," International Journal of Solids and Structures, Vol. 7, 1971, pp. 993-1005.

[15] D. B. Bogy, "Two Edge-Bonded Elastic Wedges of Different Materials and Wedge Angles under Surface Traction," Journal of Applied Mechanics, Vol.93, 1971, pp. 377-386.

[16] F. L. Mattews, P. F. Kitty, and E. W. Godwin, "A Review of the Strength of Joints in Fiber Reinforced Plastics, Part 2-Adhesively Bonded Joints," Composites, Vol. 13, No. 1, 1982, pp. 29-31.

[17] J. R. Vinson and R. L. Sierakowski, The Behavior of Structures Composed of Composite Materials (Boston: Nijhoff, 1986) pp. 239-262.

[18] F. Erdogan and M. Ratwani, "Stress Distribution in Bonded Joints," Journal of Composite Materials, Vol. 5, 1971, pp. 378-393.

[19] R. M. Barker and F. Hatt, "Analysis of Bonded Joints in Vehicular Structures," AIAA Journal, Vol. 11, 1973, pp. 1650-1654.

[20] K. L. Devries and M. L. Williams, "Adhesive Fracture of a Lap Shear Joint," Experimental Mechanics, March 1974, pp. 89-97.

[21] R. S. Alwar and Y. R. Nagaraja, "Elastic Analysis of Adhesive Butt Joints," Journal of Adhesion, Vol. 6, 1976, pp. 279-287.

[22] I. U. Ojalvo, "Optimization of Bonded Joints," AIAA Journal, Vol. 23, October 1985, pp. 1578-1582.

[23] D. W. Schmueser, N. L. Johnson and R. T. Foister, "Stress Analysis of Adhesively Bonded Electroprimed Steel Lap Shear Joints," _Journal of Adhesion_, Vol. 24, 1987, pp. 47-64.

[24] M. D. Wright, "The Stress Analysis of a Butt Strap Joint in Carbon Fiber Reinforced Plastic," _Composites_, Vol. 4, October 1978, pp. 259-262.

[25] D. J. Schwartz, "Practical Analysis of Stress Raisers in Solid Structures," _4th International Conference on Vehicle Structural Mechanics, Society of Automotive Engineers_, Warrendale, Pa., 15096, November 1981.

[26] F. S. Kelly, "Mesh Requirement for the Analysis of a Stress Concentration by the Specified Boundary Displacement Method," _Proceedings of the Second International Computer Engineering Conference_, Computer Engineering Division, ASME, August 1982.

[27] M. D. Wright, "Stress Distribution in Carbon Fiber Reinforced Plastic Joints," _Composites_, January 1980, pp. 46-50.

[28] H. L. Groth, "Calculation of Stresses in Bonded Joints Using the Substructuring Technique," _International Journal of Adhesion and Adhesives_, Vol. 6, January 1986, pp. 31-35.

[29] P. A. Gradin and H. L. Groth, "A Fracture Criterion for Adhesive Joints in terms of Material Induced Singularities," _Proceedings of the Third International Conference on Numerical Methods in Fracture Mechanics_, Pineridge Press, Swansea, 1984.

[30] U. Yuceoglu and D. P. Updike, "Comparison of Continuum and Mechanical Spring Model of Adhesive Layers in Bonded Joints," _1981 Advances in Aerospace Structures and Materials_, ASME Publication, November 1981.

[31] U. Yuceoglu and D. P. Updike, "Stress Analysis of Bonded Plates and Joints," _ASCE Journal of The Engineering Mechanics Division_, February 1980, pp. 37-56.

[32] W. S. Johnson and S. Mall, "A Fracture Mechanics Approach for Designing Adhesively Bonded Joints," _Delamination and Debonding of Materials_, STP 876, American Society for Testing and Materials, Philadelphia, 1985, pp. 189-199.

[33] G. J. DeSalvo and J. A. Swanson, <u>ANSYS Engineering Analysis System User's Manual</u>, Swanson Analysis Systems, Inc., Houston, PA., February 1982.

[35] R. D. Cook, <u>Concepts and Application of Finite Element Analysis</u>, John Wiley & Sons, New York, 1974.

[36] Yona Kaplevatsky and Vitaly Raevsky, "On the Theory of the Stress-Strain State in Adhesive Joint," <u>Journal of Adhesion</u>, 1976, Vol. 7, pp. 65-77.

[37] F. Delale, F. Erdogan, and M. N. Aydinoglu, "Stresses in Adhesively Bonded Joints: A Closed-Form Solution," <u>Journal of Composite Materials</u>, 1981, Vol. 15, pp. 249-267.

[38] R. L. Spilker and S. C. Chou, "Edge Effects in Symmetric Composite Laminates: Importance of Satisfying the Traction-Free-Edge Condition," <u>Journal of Composite Materials</u>, 1980, Vol. 14, pp. 2-20.

[39] R. L. Spilker, S. C. Chou, and O. Orringer, "Alternate Hybrid-Stress Elements for Analysis of Multilayer Composite Plates," <u>Journal of Composite Materials</u>, 1977, Vol. 11, pp. 57.

[40] S. Aivazzadeh and G. Verchery, "Stress Analysis at the Interface in Adhesive Joints by Special Finite Elements," <u>International Journal of Adhesion and Adhesives</u>, 1986, Vol. 6, pp. 185-188.

[41] Y. Yamaguchi and S. Sato, "Stress Distribution and Mechanical Strength of T- and L-type Adhesive-Bonded Joints Subjected to Applied Bending Moments," <u>International Journal of Adhesion and Adhesives</u>, 1986, Vol. 6, pp. 81-87.

[42] S. D. Conte and C. de Boor, <u>Elementary Numerical Analysis: Algorithmic Approach</u> (McGraw-Hill Book Co., 1980) pp. 202-204.

Myung Kyun Park was born December 3, 1956, in Pusan, Korea. In March 1979, he received his Bachelor of Science degree with major in mechanical engineering from the Yonsei University, Seoul, Korea. He worked for the Agency for Defense Development for five years in Korea as a mechanical engineer. In August 1984, he came to the University of Florida for graduate study in the area of solid mechanics. He received his Master of Science degree from the department of Aerospace Engineering, Mechanics and Engineering Science in December 1985. He continued his Ph.D. study in the same department. He was awarded the degree of Doctor of Philosophy in May 1990. He married Boeun in 1983 and they have a son named James.

I certify that I have read this study and that in my opinion it conforms to acceptable standards of scholarly presentation and is fully adequate, in scope and quality, as a dissertation for the degree of Doctor of Philosophy.

Lawrence E. Malvern, Chairman
Professor of Aerospace Engineering,
Mechanics and Engineering Science

I certify that I have read this study and that in my opinion it conforms to acceptable standards of scholarly presentation and is fully adequate, in scope and quality, as a dissertation for the degree of Doctor of Philosophy.
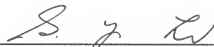
C. T. Sun
Professor of Aerospace Engineering,
Mechanics and Engineering Science

I certify that I have read this study and that in my opinion it conforms to acceptable standards of scholarly presentation and is fully adequate, in scope and quality, as a dissertation for the degree of Doctor of Philosophy.

B. V. Sankar
Assistant Professor of Aerospace
Engineering, Mechanics and
Engineering Science

I certify that I have read this study and that in my opinion it conforms to acceptable standards of scholarly presentation and is fully adequate, in scope and quality, as a dissertation for the degree of Doctor of Philosophy.

S. Y. Lu
Professor of Aerospace Engineering,
Mechanics and Engineering Science

I certify that I have read this study and that in my opinion it conforms to acceptable standards of scholarly presentation and is fully adequate, in scope and quality, as a dissertation for the degree of Doctor of Philosophy.

David C. Wilson
Professor of Mathematics

This dissertation was submitted to the Graduate Faculty of the College of Engineering and to the Graduate School and was accepted as partial fulfillment of the requirements for the degree of Doctor of Philosophy.

May 1990

Winfred M. Phillips
Dean, College of Engineering

Madelyn M. Lockhart
Dean, Graduate School